



A Worldwide and Unified Database of Surface Ruptures (SURE) for Fault Displacement Hazard Analyses

by Stéphane Baize, Fia Nurminen, Alexandra Sarmiento, Timothy Dawson, Makoto Takao, Oona Scotti, Takashi Azuma, Paolo Boncio, Johann Champenois, Francesca R. Cinti, Riccardo Civico, Carlos Costa, Luca Guerrieri, Etienne Marti, James McCalpin, Koji Okumura, and Pilar Villamor

ABSTRACT

Fault displacement hazard assessment is based on empirical relationships that are established using historic earthquake fault ruptures. These relationships evaluate the likelihood of coseismic surface slip considering on-fault and off-fault ruptures, for given earthquake magnitude and distance to fault. Moreover, they allow predicting the amount of fault slip at and close to the active fault of concern. Applications of this approach include land use planning, structural design of infrastructure, and critical facilities located on or close to an active fault.

To date, the current equations are based on sparsely populated datasets, including a limited number of pre-2000 events. In 2015, an international effort started to constitute a worldwide and unified fault displacement database (SURface Ruptures due to Earthquakes [SURE]) to improve further hazard estimations. After two workshops, it was decided to unify the existing datasets (field-based slip measurements) to incorporate recent and future cases, and to include new parameters relevant to properly describe the rupture.

This contribution presents the status of the SURE database and delineates some perspectives to improve the surface-faulting assessment. Original data have been compiled and adapted to the structure. The database encompasses 45 earthquakes from magnitude 5–7.9, with more than 15,000 coseismic surface deformation observations (including slip measurements) and 56,000 of rupture segments. Twenty earthquake cases are from Japan, 15 from United States, two from Mexico, Italy, and New Zealand, one from Kyrgyzstan, Ecuador, Turkey, and Argentina. Twenty-four earthquakes are strike-slip faulting events, 11 are normal or normal oblique, and 10 are reverse faulting.

To pursue the momentum, the initial and common implementation effort needs to be continued and coordinated, and the maintenance and longevity of the database must be guaranteed. This effort must remain based on a large and open community of earthquake geologists to create a free and open access database.

Supplemental Content: Information on the earthquakes, including date, coordinates of epicenter, focal mechanism, surface rupture information, geodesy data, information on structural context, and related references, associated shapefiles, georeferenced map file depicting the rupture sections with IDs, the complete dataset related to the surface rupture information, including basic information (IDs, references, and coordinates), horizontal and vertical components of slip, fault plane data, and site information and comments, and the associated shapefiles and a value of net slip determined from the horizontal and vertical components when not available (and hypothesis on the fault dip).

INTRODUCTION

Earthquakes are a major threat for many human activities, not only because of shaking but also because of induced surface deformation (fault-related surface ruptures). Reducing earthquake losses requires anticipating probable amplitude and location of ground motions and surface displacement. Following the extensive damage that accompanied the 1971 San Fernando, California, surface rupturing earthquake (e.g., Jennings, 1997), policy makers, engineers, and scientists have had to come to grips with the difficult task of mitigating surface rupture hazards to buildings and urban lifeline infrastructure. Anticipation of a possible major fault rupture in the design of the Trans-Alaska Oil Pipeline built in the 1970s, for example, paid off when the M_w 7.9 Denali fault earthquake ruptured the Earth's surface beneath it. The pipeline accommodated the 6 m of surface-faulting displacement suffering only minor damage, thus averting a major economic and environmental disaster. This success was due to intensive geologic investigations focused on identifying

and characterizing the Denali fault in terms of its precise location and potential displacements, emphasizing that overcoming such a threat requires geological investigations and innovative engineered mitigation. Since the 1970s, scientist know-how and survey techniques of coseismic ruptures have been developed and the quality of collected data is substantially improved, even for the detection of subtle features. This provides relatively complete scenarios for several recent earthquakes around the globe. Modern imaging and measuring techniques provide us with the chance of improving the mapping, quantification of surface rupture amplitudes in the immediate wake of events and their uncertainties. The use of terrestrial light detection and ranging (lidar) on specific spots along the M_w 7.2 El Mayor–Cucapah earthquake rupture have revealed that this technique is appropriate to estimate the uncertainties, which are difficult to assess in the field, and that apparent very irregular slip profiles could actually be caused by field choices or uncertainties (Gold *et al.*, 2013). The Interferometric Synthetic Aperture Radar (InSAR) technique was successfully used to recognize the ruptures caused by moderate earthquakes, such as the 2014 M_w 6 Napa Valley, California (DeLong *et al.*, 2016), or faint ruptures triggered by large remote events such as 2010 M_w 7.2 El Mayor–Cucapah one (Donnellan *et al.*, 2014). Optical correlation allowed the geoscientists to map and measure the extensive and complex rupture associated with the large 2016 M_w 7.8 Kaikōura, New Zealand, earthquake (Klinger *et al.*, 2018). Differential lidar has recently been used to map and measure coseismic surface faulting and deformation for the 2016 Kaikōura earthquake (Langridge *et al.*, 2018; Nicol *et al.*, 2018).

Nevertheless, to date, the absence of inclusive modern databases of earthquake ruptures covering a wide range of magnitude and various tectonic environments in a homogenous frame continues to be a significant gap. For example, surface rupture datasets from specific categories of earthquakes are still not widely and sufficiently represented. Among these are the reverse-faulting earthquakes and earthquakes of moderate magnitude, although recent earthquakes in the United States (2014 West Napa), Japan (2014 Nagano Province), and Italy (2016 Norcia) reminded us that these kind of moderate (M_w 6–6.5) events can also induce significant surface ruptures and related hazards, either on the principal (or primary) fault or secondary ruptures that are distributed around whatever the focal mechanism (Fig. 1). Improving such databases can obviously help in building more robust empirical scaling relationships between earthquake magnitude and fault displacement parameters (rupture length, average, and maximum slip), but it will also allow the analysts to substantially improve the prediction of surface-faulting likelihood and surface slip amount through *ad hoc* equations used in probabilistic approaches (namely probabilistic fault displacement hazard analyses [PFDHAs]), both for on-fault and off-fault slip, for given earthquake scenario or set of earthquakes (defined for instance by a magnitude–frequency distribution).

Actually, those predictions, derived from statistical analyses of historic ruptures datasets (Youngs *et al.*, 2003; Moss and Ross, 2011; Petersen *et al.*, 2011; Takao *et al.*, 2013), are useful when trying to predict future fault displacements at, and close to, an

active fault, and they are of special interest for structural design of infrastructure and critical facilities (e.g., Chen and Petersen, 2011).

During two recent meetings dedicated to fault displacement hazard analyses (FDHAs; Baize *et al.*, 2016; Baize and Scotti, 2017), earthquake geologists and seismic hazard practitioners shared the opinion that the surface rupture datasets and ensuing empirical relationships need to be unified, homogenized, updated, and improved. Two main outcomes from those discussions in terms of improvements of such a database are the need for: (1) aggregating the existing datasets, and (2) clearly defining the relevant parameters that should be recorded when capturing future surface rupture data and adding them to the database. In Menlo Park (2016), more than 110 earth scientists joined, representing consulting companies, governmental agencies, and researchers from the Americas, Europe, Asia, and Oceania. Potential distributed deformation appeared to be a key concern, particularly for long baseline structures; infrastructure such as pipelines cannot avoid fault traces along their paths and PFDHA becomes crucial to designing them to be resilient. There is a large use of field data in assessing hazard procedures, either at local scale with high level of accuracy for specific studies (e.g., paleoseismological trenches) or at global scale with compilation of worldwide surface rupture information.

In this article and companion material, we expose the results of a common effort to build a unified database of SURface Ruptures due to Earthquakes (SURE) to fill this gap. To our knowledge, this project represents the first and most complete effort to catalog surface rupture data in a geospatial database with associated data and metadata; it was initiated in the framework of a working group of the International Union for Quaternary Research (INQUA). Other efforts such as the University of California Fault Displacement Hazard Initiative (UC FDHI) project from the United States are in the earliest stages of database development (Sarmiento *et al.*, 2019).

OVERVIEW OF SURFACE RUPTURE PHENOMENON

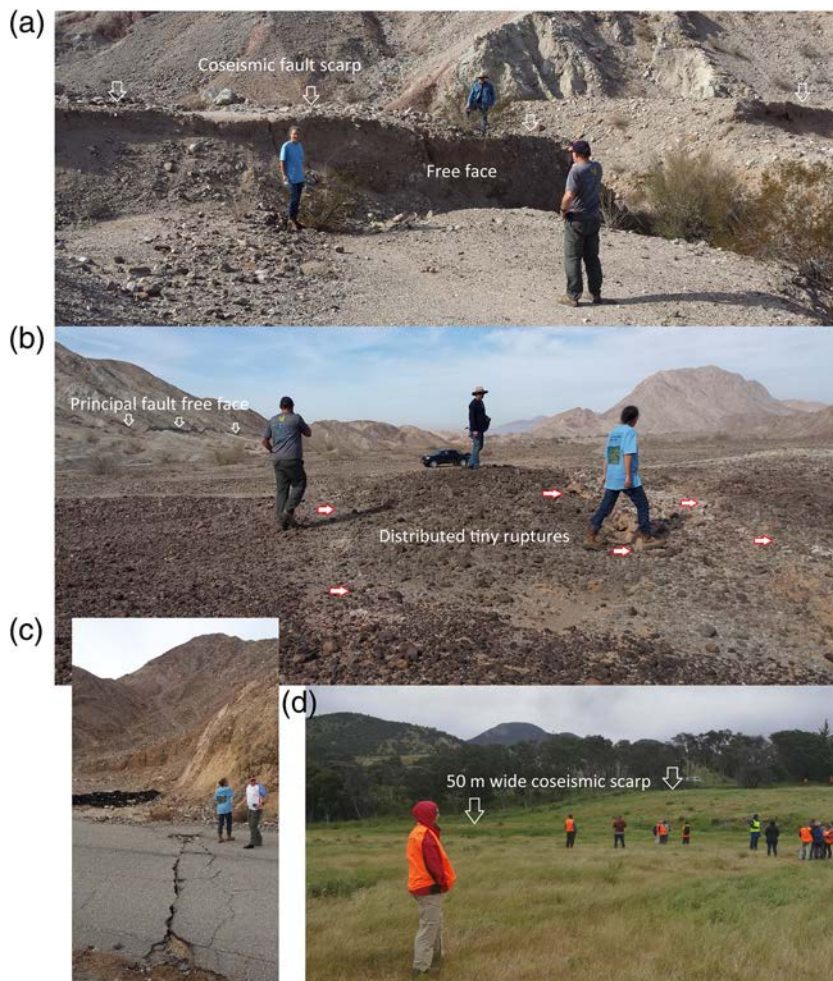
Earthquake physics states that fault source area and slip increase with energy and moment magnitude of the earthquake (Hanks and Kanamori, 1979). This is verified during the field postearthquake surveys and is statistically established by empirical scaling relationships (e.g., Wells and Coppersmith, 1994). Surface faulting is generally represented by a unique or a set of discrete surface breaks at the ground surface. The major one with the larger offsets, the longer continuity, a coherent structural arrangement, and (usually) the association with a cumulative fault, is qualified as the principal (or primary) fault (Fig. 2). In addition to clearly observable surface faulting, a fraction of warping, tilting, or folding, which can be hard to distinguish when not underlined by outstanding surfaces or piercing lines, can be present: for instance, recent striking examples arose in New Zealand during the 2010 M_w 7.1 Darfield earthquake (South Island of New Zealand) along the dextral Greendale fault (Litchfield *et al.*, 2014) and during the 2016 M_w 7.8 Kaikōura earthquake



▲ **Figure 1.** Surface ruptures related to moderate earthquakes, either on the principal or distributed (synthetic or antithetic) faults, can lead to significant damage to infrastructures and lifelines. (a,b) Surface faulting during the M_w 6.5 Norcia earthquake (30 October 2016) affected mountain roads and temporarily impeded traffic, both along (a) principal and (b) secondary antithetic segments (pictures in November 2016 and July 2017, respectively). (a) The fault offsets the new asphalt that was set up after a first damage to the road during the 24 August 2016 M_w 6 foreshock. (c–e) The roads crossing the principal fault strand that ruptured during the M_w 6 West Napa earthquake (24 August 2014) were severely damaged by (c) parallel or (d) en-*é*chelon segments, and several tiny (several centimeters) dextral offsets even damaged installations (curb and buried Pacific Gas and Electric Company pipes) crossing (e) secondary segments (pictures in December 2014). Note that panel (d) additionally illustrates the occurrence of postearthquake aseismic slip (afterslip) with the shift of the paint marks. The color version of this figure is available only in the electronic edition.

(South Island of New Zealand) with the broad flexural scarps along the reverse Papatea fault (Langridge *et al.*, 2018) (Fig. 2). Those large-aperture deformation evidences might have been unnoticed during field geological surveys as single event ruptures, especially for old historical earthquakes. Besides principal ruptures and nonlocalized deformation, off-fault secondary

ruptures are frequently described along connected splays, parallel branches (Fig. 2), or other segments structurally connected to the principal fault. Fault length, segment continuity, and slip values along distributed off-fault ruptures are typically less than those characterizing the principal fault. Minor displacements (several millimeters to several centimeters) of tectonic origin



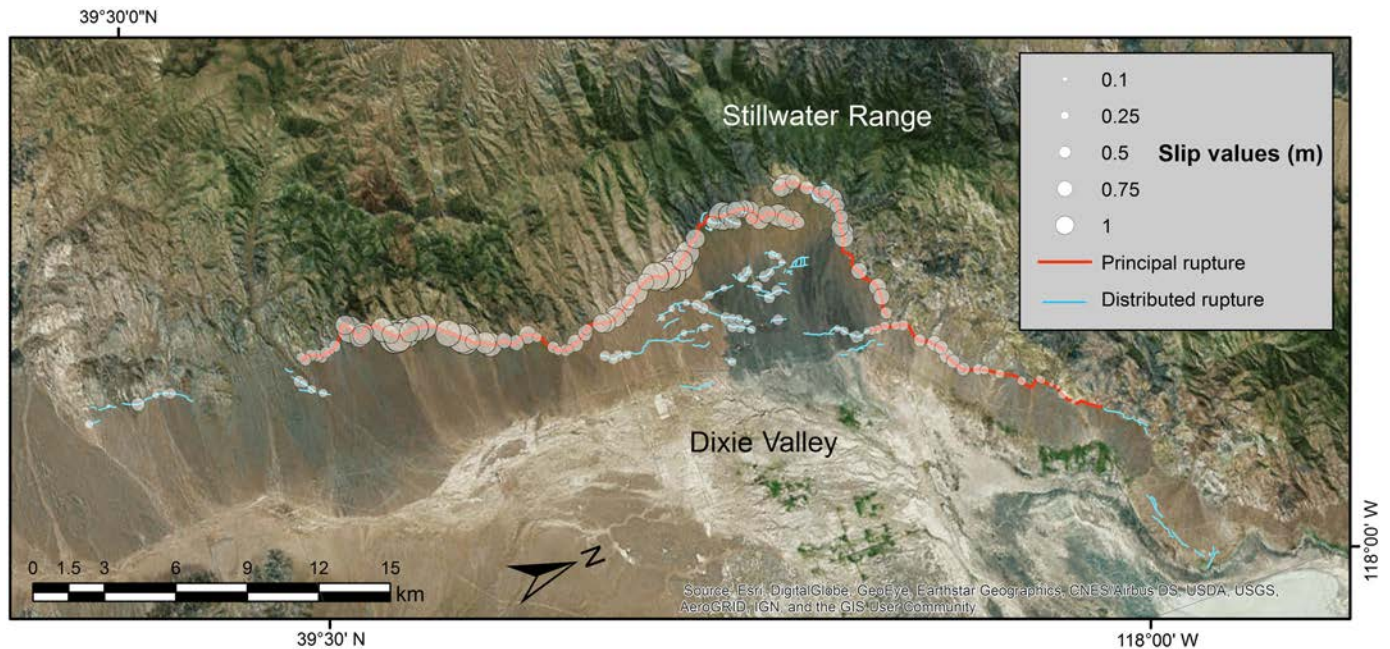
▲ **Figure 2.** Field illustration of primary and distributed faulting. (a,b) Primary faulting (open white arrows) occurred during the 6 April 2010 M_w 7.2 El Mayor–Cucapah earthquake (Mexico) along a series of east-dipping fault segments (here the Borrego segment of the El Mayor–Cucapah fault zone, with ~ 3 m of right lateral and ~ 1.5 m of normal components) and (b) off-fault ruptures with ~ 10 cm of throws were distributed over several hundred meters, sometimes along known active faults such as the (c) west-dipping Laguna Salada fault that already ruptured in 1892 and 1934. (d) Flexural shape that can characterize some reverse-faulting scarp, with the example of the ~ 8 m high and ~ 50 – 80 m wide scarp (north of Middle Hill station, between the two groups of Paleoseismicity Active Tectonics Archeoseismicity days attendees) caused by the rupture of the Papatea fault during the M_w 7.8 Kaikōura earthquake (14 November 2016). The color version of this figure is available only in the electronic edition.

have been described in remote areas along faults clearly nonconnected to the seismogenic source. At those large distances (typically several kilometers to tens of kilometers), slip is suspected to occur on active faults that are close to failure, and then governed by different physics than slip structurally connected to the earthquake source. Remote shallow and aseismic slip is possibly triggered by dynamic stress change due to seismic waves (e.g., Victor *et al.*, 2018), sometimes eventually leading to favor the nucleation of significant earthquakes (e.g., Inbal *et al.*, 2017). Such triggered slip occurred, for instance, on historically active faults of southern California as a consequence of the 2010 M_w 7.2 El

Mayor–Cucapah earthquake in northern Mexico, at distances exceeding 100 km (Rymer *et al.*, 2011; Wei, Fielding, *et al.*, 2011).

The characteristics of the near-surface geology influences the pattern of surface rupture, as exemplified by the 2010 El Mayor–Cucapah, Mexico, strike-slip to normal-oblique faulting earthquake (Teran *et al.*, 2015). This changing pattern with surface geology has long and largely been documented over the world, whatever the focal mechanism of the earthquake and the kinematics of the surface fault (e.g., M_w 7.9 Wenchuan reverse-faulting earthquake; Yu *et al.*, 2010, or M_w 7.7 Balochistan strike-slip earthquake; Vallage *et al.*, 2015). Sandbox models confirm the importance of understanding the near-surface material properties to predict the pattern and distribution of surface deformation at a study site. In those experimental results, the near-surface material stiffness and the tectonic history are crucial parameters that control the rupture pattern and fabric (Stanton, 2013; Moss *et al.*, 2018). In the database, we propose to introduce the surface geology parameter for implementation of future events. If enough data are gathered, specific regressions for each near-surface geology type might be developed. The structural arrangement of the principal fault is another factor that conditions deformation distribution. Whether the fault is represented by unique or simple traces, or presents irregularities, the off-fault deformation will vary in nature, distribution, and amount. The occurrence of bends, stepovers, jogs, fault sinuosity, and a position at a fault tip will enhance the distribution of deformation as evidenced by historical cases (1979 Imperial Valley or 2010 El Mayor–Cucapah earthquakes). An iconic case is the 1954 M_w 7+ Dixie valley surface rupture that broke one of the Basin and Range normal faults: from south to north, the principal fault, with offsets of about a meter along the cumulative fault at the base of the slope, forms an ~ 12 km bend in which numerous, discontinuous, and small offset faults affect

the hanging wall (Fig. 3, data from Caskey *et al.*, 1996). In reverse-faulting earthquake cases, surface deformation can present peculiar secondary deformation features (bending-moment ruptures, flexural-slip ruptures) when associated with coseismic fault-related folding, as evidenced for instance after the M_w 7 El Asnam (Algeria) earthquake in 1980 (Philip and Meghraoui, 1983). To account for those particularities, we propose to assign to the principal and secondary faulting evidences an attribute describing the corresponding pattern of principal rupture, either continuous and linear (regular) portion, complex (stepovers, gaps, relays, and fault tip), or revealing any



▲ **Figure 3.** Map of the primary and distributed ruptures during the Dixie Valley earthquake (1954). Data compiled by Pezzopane and Dawson (1996) from the Caskey *et al.* (1996) publication. The color version of this figure is available only in the electronic edition.

other relevant structural feature (fault-related fold, graben, and parallel bedrock faulting). In addition, because of the significant impact of the position relative to rupture plane at depth (mainly in dip-slip cases) and related hazard (e.g., Youngs *et al.*, 2003; Boncio *et al.*, 2018), the data description will account for the hanging wall or footwall location of distributed ruptures. When deriving empirical relationships, those parameters may be analyzed separately and/or be used to develop regressions that are specific to the type of fault section.

Earthquake surface rupture commonly occurs along long-living geological structures with a documented historical and/or prehistorical activity, both at plate boundaries (e.g., 1906 M_w 7.5+ San Francisco earthquake along the San Andreas fault; Schwartz *et al.*, 2014) and along less active faults such as those in central Italy where severe damages can also occur: during the 2009 M_w 6.3 L'Aquila (Cinti *et al.*, 2011), although coseismic surface offsets were in the order of few centimeters, the rupture trace crossed and broke apart an urban lifeline infrastructure, the Gran Sasso water pipeline. In Figure 4, we depict as an example the case of the 22 November 2014 M_w 6.2 earthquake in central Japan along the Kamishiro where Okumura (2001) evidenced at the place of the 2014 rupture a series of paleoearthquakes. Because slip history of ruptured faults is potentially a relevant topic for inferring future surface rupturing events, the SURE database allows the implementation of paleoseismological information.

DATA COLLECTION

General Comments

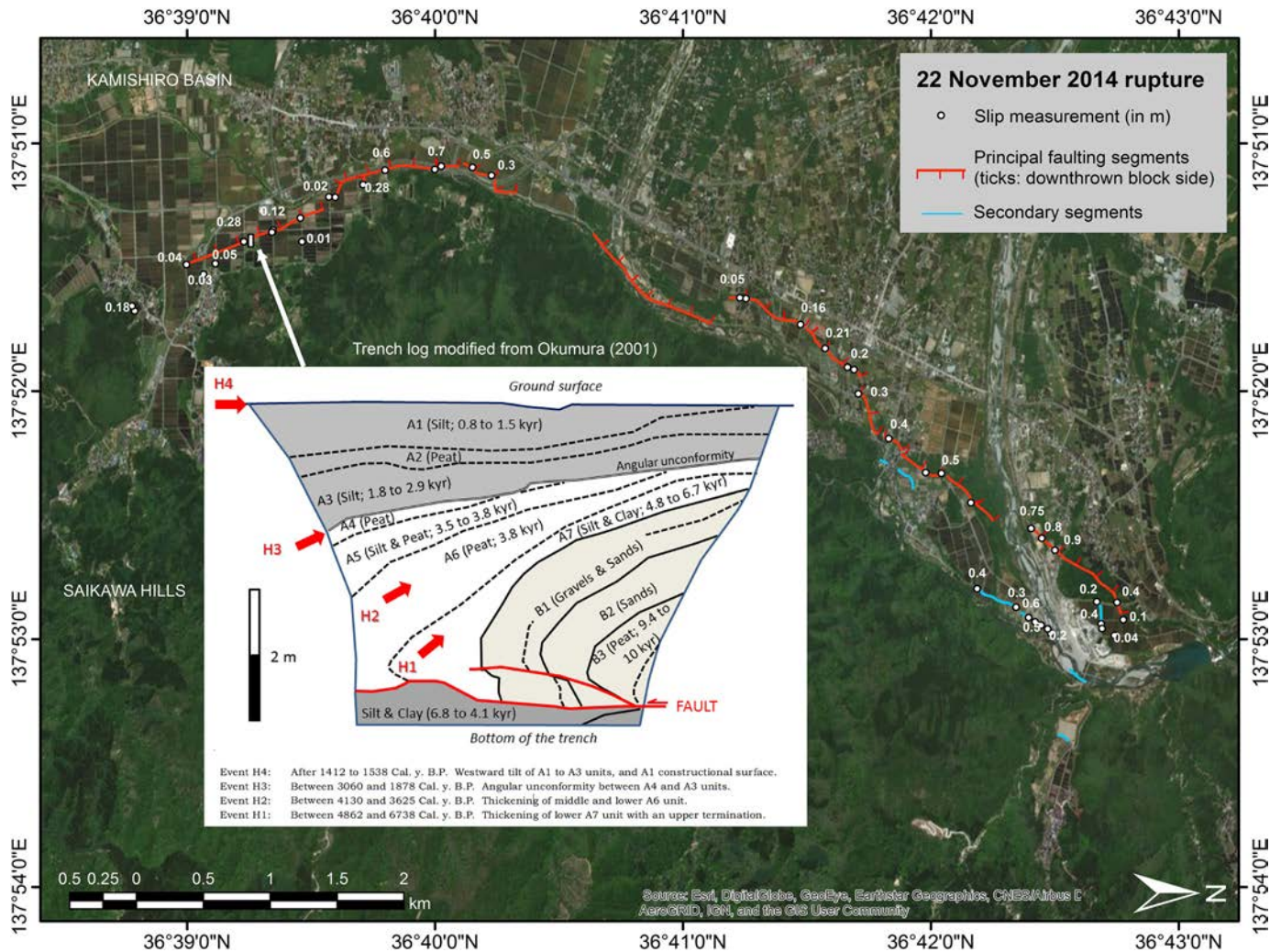
The surface rupture database, as a first step to future prediction equations of surface-faulting occurrence and amount of slip,

would be developed by accounting for all the relevant parameters such as location, geometry, slip amount, and kinematics. It is therefore containing geospatial information gathering field measurements captured during postseismic surveys, in the form of segment maps and slip measurement tables. The compilation of existing information herein consisted of aggregating surface rupture cases already merged in various datasets and gathering publications with sufficient and appropriate data measured in the field.

To produce a unified database, variable amounts of editing, drawing, and interpretation were required because information comes from a large variety of authors (and then diversity of utilized terminology) and of field conditions. Therefore, a careful reading of the referenced dataset was undergone to properly transfer the reported data into the unified SURE structure and following the nomenclature used for reporting the surface fault displacement and shown in Figure 5. We tried to keep track of the initial identification index when possible. The reported surface rupture information has been compiled at Institut de Radioprotection et de Sûreté Nucléaire (IRSN) and Institut du Physique du Globe de Paris (IPGP), France.

Database Structure

The SURE database is basically built on three-component files, describing the earthquakes, the rupture sections, and the slip observations. The information is contained in Tables 1, 2, and 3, in which numerical values are stored respectively for earthquakes and slip observations, associated with corresponding geospatial vector data (shapefiles), and in rupture sections' shapefile. All these files are provided in the supplemental content to this article. In the slip observations shapefile, we report a net slip value computed from the horizontal and vertical



▲ **Figure 4.** Surface rupture of the 2014 Nagano Prefecture earthquake (data from [Katsube et al., 2017](#)) crosscut a site where paleo-earthquakes were exposed in a trench. Inset shows the so-called Hakuba trench section modified from [Okumura \(2001\)](#); ages are given in calibrated years before present (cal. yr B.P.). [Okumura \(2001\)](#) evidences four paleoearthquakes (H1 to H4) from the geometrical properties of layers, such as thickening of A7 (H1) and of A6 (H2), angular unconformity between A4 and A3 (H3), and the tilt of A1 to A3 (H4). The color version of this figure is available only in the electronic edition.

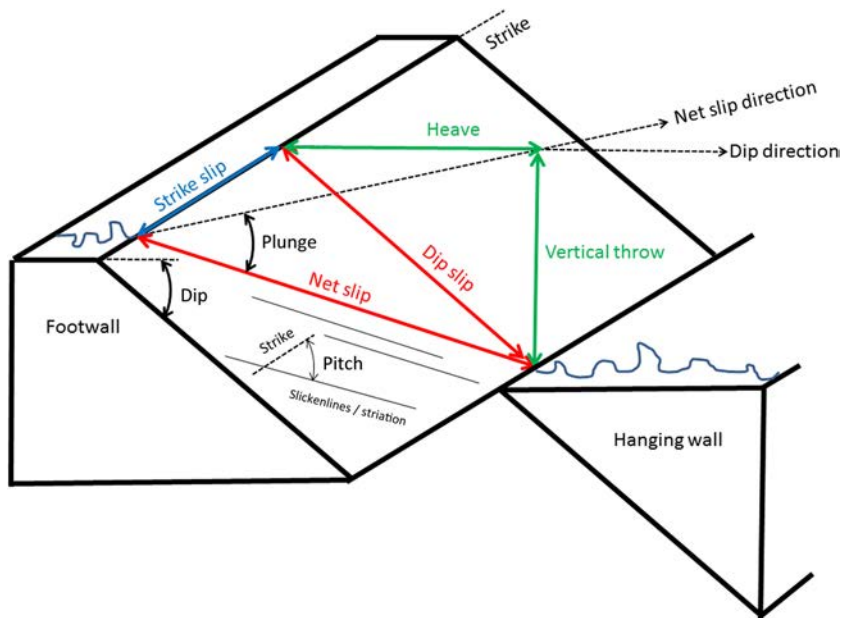
components of displacement; for vertical, we used the scarp heights or vertical throw, and the fault dip (when available).

Most of the seismological parameters for the earthquakes (identified by IdE) have been compiled from the International Seismological Centre-Global Earthquake Model (ISC-GEM) earthquake catalog ([International Seismological Centre-Global Earthquake Model \[ISC-GEM\] Earthquake Catalogue, 2019](#)), including moment magnitudes and depths. Overall estimation of surface rupture length, maximum and average displacement are grabbed in the source article or other reference; seismotectonic context corresponds to a short definition of the tectonics of the area inferred from the literature; geodetical or seismological information often refers to a link to the SRCMOD ([Mai and Thingbaijam, 2014](#)) database that aggregates and synthesizes published models. Relevant information about paleoearthquake and slip history is documented based on published articles.

Attributes in the rupture sections shapefile are the IdE of the causative earthquake and the ID of the segments (Ids).

The complete rupture map (on- and off-fault ruptures) is an important part of the database because this information is used to calculate the conditional probability of rupture in PFDHA ([Youngs et al., 2003](#); [Petersen et al., 2011](#)).

The slip observations table includes, beside basic information, slip measurement and fault information (Table 3). Net slip is rarely reported in source articles or studies. Keeping track of the horizontal and vertical components can be important because engineers could necessitate this information to properly design a building or a facility. For instance, a strategy to mitigate dip-slip rupture could be to build on top of ductile earth fills that could deviate or prevent the underlying fault to reach the earth surface ([Oettle and Bray, 2013](#)). In case of lateral motions, engineers decided to lay the Trans-Alaska

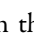


▲ **Figure 5.** Convention used to describe the surface rupture metrics and parameters. Reported terms are commonly admitted words that describe the fault kinematics both in structural or neotectonic studies. The color version of this figure is available only in the electronic edition.

pipeline on horizontal beam sliders parallel to the fault, so that the structure could accommodate the 2002 Denali rupture (see [Data and Resources](#)). In the shapefile related to the slip dataset, we report a net slip value for the complete set of points, which has been calculated from horizontal and vertical components in most cases. The table allows the implementation of large aperture offset, which sums up the discrete slip on the fault trace and the off-fault part of deformation that can occur at tens to hundreds of meters. The database is also suited for gathering information about structural complexity of primary fault near the identification number of the slip observation (IdO), and about local surface geology; this huge work has not been done yet. Any additional and relevant information can be indicated in the comment row.

Each individual slip data (IdO) and rupture segment (IdS) are linked to the causative earthquake (IdE). At the end, the tables can easily be joined and the database could be processed through Structured Query Language requests. In the database, IdO indexes are associated with the original Id defined by the data authors (when available).

DATA QUALITY AND COMPLETENESS

The data are made available in the  supplemental content. To date, the effort focused on aggregating the existing datasets (pre-2010 events) and on enriching the database with very recent cases. Some of the 45 earthquake surface ruptures correspond to historical events (back to the nineteenth century) and were mapped either soon after or very recently; in any case, their information might be biased by large uncertainties, errors, and incompleteness. Other cases (e.g., 2014 West Napa,

United States, and 2016 Norcia, Italy, earthquakes) were rapidly surveyed by many geologists with the aim of capturing the complete information of ground deformation, combining classical field measurement (tape, compass, and Real Time Kinematic Global Positioning System) or modern high-resolution techniques (lidar, structure from motion) and could be considered to cover a substantial completeness.

A big part of the dataset is not yet filled out in the tables, including the local geological information and structural complexity that are critical criteria influencing rupture arrangement and amplitude, and which potentially could be utilized to derive specific empirical relationships. Completing this work is a challenge for the coming years, as well as ranking (principal vs. distributed faulting) each individual rupture.

Key long-term goals for having further reliable and comprehensive empirical relationships also include incorporating data derived from the modern high-resolution techniques. The modern measurement techniques provide richer observation datasets of surface deformation, with high-measurement density both along faults and

perpendicular to faults, and these data will improve predictions of strain distribution and fault displacements. The U.S. community recently initiated a multiyear study that aims to develop a database combining field and geodetic measurements of earthquake-related surface faulting, to be used in surface-faulting hazard analyses in the western United States ([Sarmiento et al., 2019](#)). The group of worldwide geologists who joined the SURE community should clearly take advantage of this momentum and interact through collaboration and coordination of efforts with the U.S. community.


Ensuring that the database includes earthquakes from all known seismotectonic environments is an important component for developing models that are able to predict fault displacement. For example, there is a paucity of displacement data in the SURE database for the Asian continent; however, a basic search in the U.S. Geological Survey (USGS) database of post-2000 $M_w > 6$ crustal earthquakes reveals most of these events are located in Asia, including China, Taiwan, Japan, the Philippines, Myanmar, Russia, Iran, Kyrgyzstan, Pakistan, Turkey, and very few have documented information on surface rupture in the literature. The search for new contributors will be one major task to improve the SURE database in the next years.

INITIAL CONTENT OF THE DATABASE

Numerous slip distributions along the primary faults are available in the literature (e.g., [Lettis et al., 1997](#); [Hemphill-Haley and Weldon, 1999](#); [Wesnously, 2008](#)), but a limited number of earthquake cases yield information on distributed faulting off the primary rupture (e.g., [Pezzopane and Dawson, 1996](#); [Petersen et al., 2011](#); [Takao et al., 2013](#); [Boncio et al., 2018](#)).

Table 1
Earthquake Information

ID	IdE	Concatenation of earthquake date numbers yyyy/mm/dd	
	Name	Usual name of the earthquake	
Earthquake parameters Earthquake parameters and surface rupture	Fault system name	From bibliography, if any	
	Year	YYYY	
	Month	mm	
	Day	dd	
	Name	For instance, name by or according to literature (see Data and Resources)	
	Region	Country or Flinn–Engdahl regionalization	
	M_w	From ISC catalog or alternative source (recent events)	
	Longitude	Decimal degrees	
	Latitude	Decimal degrees	
	Depth	From ISC catalog or alternative source (for most recent events)	
Surface rupture, and deep rupture	Focal mechanism (and related reference)	Reverse, normal, strike-slip, oblique	
	SRL, MD, AD from Geology investigations (and related reference)	Data from literature	
	Geodesy information	GNSS, InSAR, or other geodesy data provide insight on coseismic surface deformation	
	References	Data from literature (geodesy or seismology inversion)	
	Seismological layer thickness	Data from CRUST1.0 model	
	Structural context	Explain briefly the structural background of the seismicity (e.g., Basin and Range, Fold-and-Thrust range, Intraplate)	
	Inversion tectonics	Yes/no	
	Morphoclimatic context	Explain the basic context in terms of climatic terms (e.g., Köppen–Geiger classification)	
	Fault history	Paleoearthquakes	Describe briefly the paleoseismological record
		Slip rate	From literature, if any
Original data	Source of data for implementation	Reference(s)	
	Description of implementation process and map scale	Text	

Earthquake information on selected events is given in the  supplemental content. Each earthquake is known through an ID (IdE), which is built following the format yyyy/mm/dd. One exception in the current database is the Dixie Valley earthquake, which happened exactly the same day as the Fairview Peak event: the former has been assigned a yyyyymm(dd+1) IdE. AD, average displacement; GNSS, Global Navigation Satellite Systems; InSAR, Interferometric Synthetic Aperture Radar; ISC, International Seismological Centre; MD, maximum displacement; SRL, surface rupture length.

In all cases, the datasets include limited descriptions of the ruptures, together with georeferenced slip measurements.

The surface rupture dataset of [Pezzopane and Dawson \(1996\)](#) encompasses 13 normal-faulting events with distributed faulting occurrences. The strike-slip event dataset in [Petersen *et al.* \(2011\)](#) contains nine events with earthquake magnitude ranging from 6.5 to 7.6, whereas the [Takao *et al.* \(2013\)](#) dataset contains 18 earthquakes from Japan (reverse and strike-slip mechanisms). The reverse surface rupture database compiled by [Moss and Ross \(2011\)](#) does not include any information on distributed ruptures, whereas [Boncio *et al.* \(2018\)](#) compiled distributed rupture information for nonsubduction reverse

earthquakes to derive criteria for fault zoning and avoidance; most of those last are still to be included.

To date, 45 earthquakes make up SURE in the M_w 5–7.9 magnitude range, including 20 cases in Japan, 15 in the United States, two in Mexico, Italy, and New Zealand, one in Kyrgyzstan, Ecuador, Turkey, and Argentina. Twenty-four earthquakes are strike-slip faulting events, 11 are normal or one normal-oblique, and 10 are reverse faulting. The dataset includes more than 15,000 surface rupture observations (including slip measurements), and more than 56,000 rupture sections.

The 45 events (Table 4) arise from three major contributions:

Table 2
Rupture Section Information

ID	IdE	Concatenation of earthquake date numbers yyyy/mm/dd
	IdS	Iterative number
Fault section parameters	Fault section name	From literature, if any
	Length	In kilometers; provided by field observer or calculated under GIS
	Strike	In degrees; provided by field observer
	Dip	In degrees; provided by field observer
Surface geology	Cover bed	b/b rupture in bedrock, b/s rupture between bedrock and sediments, s/s rupture in sediments
Structural pattern	Fault pattern complexity (regular or complex)	Describe the observation site location with respect to pattern of the principal fault trace, for example, regular principal fault or complex pattern, such as fault tip, bend, gap, stepover or coseismic fold
	Hanging wall vs. footwall	Describe the relative location of observed distributed slip with respect to principal fault plane
Fault history	Paleoearthquakes	Describe briefly the paleoseismological record
	Slip rate	From literature, if any

To date, the information on rupture section is only represented by a shapefile and its attribute file with IdS (© supplemental content). In the future, several additional data could be added. During the construction of the database skeleton, the working group suggested incorporating information about the fault sections (name, length, strike, etc.) of the fault system (if any), to which observations could be related. When a fault section (IdS, fault section name) has been studied through paleoseismological investigations, it is relevant information to indicate its slip rate, the occurrence of paleoearthquakes displacements, and their recurrence. GIS, Geographic Information Systems.


- [Petersen et al. \(2011\)](#): seven earthquakes (out of nine) strike-slip faulting earthquakes, which occurred between 1968 and 1999, are in the 6.5–7.6 magnitude range and include principal and distributed slip information. Original data are from [Clark \(1972\)](#) for 1968 Borrego earthquake in the western United States, [Sharp et al. \(1982\)](#) for 1979 M_w 6.5 Imperial Valley, ([Sharp et al., 1989](#)) for 1987 M_w 6.7 Superstition Hills, [Hart et al. \(1993\)](#) for 1992 M_w 7.2 Landers, [Treiman et al. \(2002\)](#) for 1999 Hector Mine, and [Barka et al. \(2002\)](#); [Hartleb et al. \(2002\)](#) and [Langridge et al. \(2002\)](#) for 1999 M_w 7.2 İzmit. The 1999 Kobe earthquake data were taken from the [Takao et al. \(2013\)](#) database, not from [Petersen et al. \(2011\)](#).
- [Pezzopane and Dawson \(1996\)](#): this report provides data about normal-faulting earthquakes in the western United States and nearby Mexico extensional Basin and Range province, with 1872 Owens Valley ([Beanland and Clark, 1994](#)), 1915 Pleasant Valley ([Wallace, 1984](#)), 1954 Dixie Valley and Fairview Peak ([Caskey et al., 1996](#)), 1959 Hebgen Lake (mainly in [Myers and Hamilton, 1964](#)), 1980 Mammoth Lake ([Clark et al., 1982](#)), and 1983 Borah Peak ([Crone et al., 1987](#)). We digitized the fault maps and reported the offset values produced by those authors for these earthquakes.
- [Takao et al. \(2013\)](#): the 18 strike-slip and reverse earthquakes, which original data come from references in Japanese, are in the 6–7.4 magnitude range. Some historical events date back to the nineteenth century and are poorly documented; others (e.g., 1995 Kobe) contain detailed information on primary and off-fault slip.

The database contains other cases from the literature as well such as the following earthquakes: 1887 M_w 7.5 Sonora, Mexico ([Suter, 2015](#)), 1911 $M_w \sim 7.7$ Chon-Kemin, Kyrgyzstan ([Arrowsmith et al., 2017](#)), 1971 M_w 6.7 San Fernando, United States ([Bonilla et al., 1971](#); [Kamb et al., 1971](#)), 1987 M_w 6.7 Edgecumbe, New Zealand ([Beanland et al., 1989](#)), 2002 M_w 7.9 Denali ([Haeussler et al., 2004](#)), 2010 M_w 7 Darfield, New Zealand ([Quigley et al., 2012](#); [Villamor et al., 2012](#); [Litchfield et al., 2014](#)), 2010 M_w 5 Pisayambo, Ecuador ([Champenois, Baize, et al., 2017](#)), 2014 M_w 6.3 Nagano, Japan ([Katsube et al., 2017](#)), and Napa, California ([Ponti et al., 2019](#)), 2016 M_w 7 Kumamoto, Japan ([Shirahama et al., 2016](#)), and M_w 6.5 Norcia, Italy ([Civico et al., 2018](#); [Villani et al., 2018](#); [Brozzetti et al., 2019](#)) earthquakes. It is relevant to specify that the dataset of the latter probably cumulates the ruptures and displacements of the 24 August M_w 6.0, 26 October M_w 5.9, and 30 October M_w 6.5 earthquake sequence, as the geologists could not separate systematically the contribution of the M_w 6.5 mainshock from previous events. We also included datasets that are not reported in peer-review articles such as the 1944 La Laja, Argentina ([Castellanos, 1944](#)) and 2009 L'Aquila ([Cinti et al., 2018](#)) earthquakes.

The database will be rapidly enriched with the recently published datasets of the 2016 M_w 7.8 Kaikōura, New Zealand, earthquakes ([Kearse et al., 2018](#); [Langridge et al., 2018](#); [Litchfield et al., 2018](#); [Nicol et al., 2018](#); [Williams et al., 2018](#)), and of other reverse-faulting earthquakes already prepared by [Boncio et al. \(2018\)](#) in the form of shapefiles and tables. The 1905 and 1957 $M_w \sim 8$ events in Mongolia, which have been documented in

Table 3
Slip Observation Information

Basic information	IdE	Concatenation of earthquake date numbers yyyy/mm/dd
	IdS	Segment ID
	IdO	Observation of rupture ID
	Date	Date of observation
	Initial reference	Source of data
	Observer	Name
	Id observer	ID provided by observer
	Longitude	In decimal degrees (WGS84)
	Latitude	In decimal degrees (WGS84)
	Elevation	In meters
Horizontal component of fault displacement	Strike slip (SS)	Horizontal component of discrete slip along fault plane (in meters)
	Sense of slip (SS)	LL, left lateral; RL, right lateral
	Uncertainty horizontal (\pm) (SS)	In meters
	Maximum and minimum values (SS)	In meters
	Large-aperture offset (SS) and uncertainty	Corresponds to the total strike component of fault displacement, including that on the discrete fault plane and off-fault flexure, if any (in meters)
	Aperture width (SS)	Width of the band in which large-aperture offset is accommodated (in meters)
	Fault-normal component (heave) (FNS) and sense of relative displacement	Shortening (S) or lengthening (L) (in meters)
Vertical component of fault displacement	Opening	Aperture of the rupture measured perpendicular to the walls (in meters)
	Vertical throw (VT) (m)	Separation between hanging wall and footwall measured vertically (in meters)
	Upside	Gives the cardinal direction of the upthrown block surrounding the fault
	Uncertainty vertical (\pm) (VT)	In meters
	Maximum and minimum vertical (VT)	In meters
	Large-aperture offset (VT) (m) and uncertainty	Corresponds to the total vertical component of fault surface displacement (throw), including that on the discrete fault plane and off-fault flexure, if any (in meters)
	Aperture width (VT)	Width of the band where large-aperture offset is accommodated (in meters)
	Vertical slip (VS) (m) and uncertainties	Free-face fault slip and actual vertical component of slip, accounting for the fault dip (in meters)

In the shapefile attribute file, we report longitude and latitude in decimal degrees, referenced in the World Geodetic System of 1984 (WGS84) geographic coordinates system, net slip values in meters and the surface geology for few events. More complete data are provided in the  supplemental content. In some cases, the net slip value has been directly reported by the authors; however, in most cases, value of slip along fault strike and vertical throw of coseismic slip are provided. Actual vertical component of slip (dip slip) has been obtained by fixing an arbitrary vertical dip when value is not specified. The dataset as well includes information about heave (i.e., horizontal component of relative displacement perpendicular to fault), with negative ones when lengthening and positive ones when shortening. The displacements are given in absolute values. Sense of displacement is given separately, in a specific column. Few cases have detailed information on fault azimuth and dip. The table allows the further implementation of large aperture offset, which sums up the discrete slip on the fault trace and the inelastic part of deformation that can occur at tens to hundreds of meters (see an illustration of that in [Kearse et al., 2018](#)), and for structural complexity. Uncertainties can be reported in two ways: either with maximum and minimum values or with preferred (central) value and (\pm). When disposing of max and min, we calculate the mean to report the offset. FNS, fault normal slip.

(Continued next page.)

Table 3 (continued)
Slip Observation Information

Total fault displacement	Net slip (NS) (m) and uncertainties	In the slip_obs shapefile, we provide an NS value, either from measurement or from calculation based on horizontal and vertical components (in meters)
	Net slip (NS) direction	Direction (0°–360°) of the net slip vector
	Large aperture net slip (NS) (m)	Corresponds to the total offset of surface displacement, including on the discrete fault plane and off-fault flexure, if any (in meters)
	Plunge	Angle between the horizontal plane and the Net slip vector (°). Also called slip vector inclination
	Pitch	Angle between strike and slip vector measured in the fault plane (°). Also called Rake
Fault parameters	Strike	Fault strike with uncertainties or maximum and minimum values (in degrees)
	Dip	Fault plane dip, with uncertainties or max. and min. values. In degrees. If not given, we assume 90° (to calculate the net slip)
Surface geology	Cover bed	b/b when rupture in bedrock, b/s when rupture between bedrock and sediments, s/s when rupture in sediments, h when rupture observed across human-made features
	Cover nature—lithology	Alluvium, colluvium, lacustrine, etc., and clay, sands, gravels, soil, calcrete, etc.
	Thickness	Thickness of cover bed sediments (in meters)
Structural pattern	Fault pattern complexity	Describe the observation site location with respect to pattern of the principal fault trace, for example, regular principal fault or complex pattern, such as fault tip, bend, gap, stepover or coseismic fold
	Hanging wall vs. footwall	Describe the relative location of observed distributed slip with respect to principal fault plane
Morphologic context	Local slope (%)	Value of slope at observation location
	Location in topography	Relative location with respect to local topography (i.e., top of slope, base level, etc.)
	Water table depth	In meters
Comment		Any relevant information

In the shapefile attribute file, we report longitude and latitude in decimal degrees, referenced in the World Geodetic System of 1984 (WGS84) geographic coordinates system, net slip values in meters and the surface geology for few events. More complete data are provided in the [supplemental content](#). In some cases, the net slip value has been directly reported by the authors; however, in most cases, value of slip along fault strike and vertical throw of coseismic slip are provided. Actual vertical component of slip (dip slip) has been obtained by fixing an arbitrary vertical dip when value is not specified. The dataset as well includes information about heave (i.e., horizontal component of relative displacement perpendicular to fault), with negative ones when lengthening and positive ones when shortening. The displacements are given in absolute values. Sense of displacement is given separately, in a specific column. Few cases have detailed information on fault azimuth and dip. The table allows the further implementation of large aperture offset, which sums up the discrete slip on the fault trace and the inelastic part of deformation that can occur at tens to hundreds of meters (see an illustration of that in [Kearse et al., 2018](#)), and for structural complexity. Uncertainties can be reported in two ways: either with maximum and minimum values or with preferred (central) value and (\pm). When disposing of max and min, we calculate the mean to report the offset. FNS, fault normal slip.

terms of surface rupture with extensive description and slip measurements earthquakes, are available in detail in tables and Google Earth files ([Choi et al., 2018](#); [Kurtz et al., 2018](#)).

FUTURE EVOLUTION OF THE SURE DATABASE

Contribution of High-Resolution Techniques

Modern field, Synthetic Aperture Radar (SAR), lidar, and photogrammetric datasets contain a dense array of measurements

that capture primary and secondary rupture locations and, with the appropriate approaches, those high-resolution techniques are useful to quantify distributed deformation. These techniques, in part or in whole, have been applied recently to several earthquakes and have significantly improved geologists' abilities to map and measure surface rupture and deformation associated with moderate events (e.g., 2014 M_w 6 West Napa earthquake), earthquakes in remote or highly vegetated areas (e.g., 2010 M_w 5 Pisayambo, Ecuador). Quantifying the

Table 4
Main Characteristics of the 45 Earthquakes Included in the SURE Database

IdE*	yyyy/mm/dd	Name	Region	M_w	Longitude (°)	Latitude (°)	Depth (km)	FM†
18720326	1872/03/26	Owens lake	U.S.A.	7.45	-118.1	36.65		SS
18870503	1887/05/03	Sonora	Mexico	7.5	-109.25	30.8		N
18911028	1891/10/28	Nobi	Japan	7.4	136.6	35.6	10	SS
18960831	1896/08/31	Rikuu	Japan	6.7	140.7	39.5	10	R
19110103	1911/01/03	Chon-Kemin	Kazakhstan/Kyrgyzstan	7.7	78.53	43.013	20	R
19151003	1915/10/03	Pleasant Valley	U.S.A.	6.8	-117.654	40.258	10	N
19181111	1918/11/11	Omachi	Japan	6.4	137.3	36.1	10	R
19270307	1927/03/07	North Tango	Japan	7.1	135.0129	35.6317	10	SS
19301125	1930/11/25	North Izu	Japan	6.9	139.1295	35.0497	15	SS
19380529	1938/05/29	Kussharo	Japan	5.8	145.0109	42.9999	0	SS
19390501	1939/05/01	Oga	Japan	7	139.771	39.979	10	SS
19430910	1943/09/10	Tottori	Japan	7	133.9932	35.4481	15	SS
19440115	1944/01/15	La Laja	Argentina	7.2	-68.491	-31.496	15	R
19450112	1945/01/12	Mikawa	Japan	6.7	137.0638	34.6123	10	R
19541216	1954/12/16	Fairview Peak	U.S.A.	7.1	-117.981	39.346	10	N
19541217	1954/12/16	Dixie Valley	U.S.A.	6.6	-117.704	39.207	15	N
19590130	1959/01/30	Deshibori	Japan	6	144.5088	43.3708	25	SS
19590818	1959/08/18	Hebgen Lake	U.S.A.	7.2	-110.891	44.63	10	N
19680409	1968/04/09	Borrego Mountain	U.S.A.	6.6	-116.234	33.058	10	SS
19710209	1971/02/06	San Fernando	U.S.A.	6.7	-118.4126	34.2740	8.4	R
19740508	1974/05/08	Izu peninsula Bay	Japan	6.4	138.753	34.5719	10.3	SS
19780114	1978/01/14	Izu Offshore	Japan	6.6	139.2254	34.8023	24.4	SS
19791015	1979/10/15	Imperial Valley	U.S.A.	6.5	-115.374	32.752	10	SS
19800525	1980/05/25	Mammoth lake	U.S.A.	6.2	-118.908	37.53	10.2	N
19831028	1983/10/28	Borah Peak	U.S.A.	6.9	-113.796	44.092	10	N
19840913	1984/09/13	Nagano Prefecture	Japan	6.2	137.4871	35.7824	17.9	SS
19870302	1987/03/02	Edgcumbe	New Zealand	6.5	176.80	-37.89	10	N
19871124	1987/11/24	Superstition Hills	U.S.A.	6.5	-115.886	33.011	10	SS
19920628	1992/06/28	Landers	U.S.A.	7.3	-116.557	34.188	10	SS
19950116	1995/01/16	Hyogo Prefecture	Japan	6.9	135.0409	34.554	19	SS
19980903	1998/09/03	Iwate Prefecture	Japan	5.8	140.7555	39.743	7.6	R
19990817	1999/08/17	İzmit	Turkey	7.6	29.979	40.807	15	SS
19991016	1999/10/16	Hector Mine	U.S.A.	7.1	-116.387	34.539	20	SS
20001006	2000/10/06	Tottori Prefecture	Japan	6.7	133.157	35.38	0.6	SS
20021103	2002/11/03	Denali	U.S.A.	7.9	-147.597	63.512	12.5	SS
20041023	2004/10/23	Niigata Prefecture	Japan	6.6	138.7706	37.3032	8.5	R
20080613	2008/06/13	Iwate-Miyagi	Japan	6.9	140.7365	39.1514	11.6	R
20090406	2009/04/06	L'Aquila	Italy	6.3	13.353	42.368	10	N
20100326	2010/03/26	Pisayambo	Ecuador	5	-78.32	-1.24	10	SS
20100404	2010/04/04	El Mayor	Mexico	7.2	-115.266	32.348	10	O
20100903	2010/09/03	Darfield	New Zealand	7.2	172.17	-43.53	11	SS
20140824	2014/08/24	Napa	U.S.A.	6	-122.312	38.215	11.1	SS
20141122	2014/11/22	Nagano Prefecture	Japan	6.2	137.888	36.641	9	R
20160415	2016/04/15	Kumamoto	Japan	7	130.77	32.84	12.9	SS
20161030	2016/10/30	Norcia	Italy	6.5	13.1107	42.8322	9.2	N

SURE, SURface Ruptures due to Earthquakes.

*Identifying number of the earthquake.

†Focal mechanism of the earthquake.

magnitude and spatial distribution of off-fault deformation produced during earthquakes is now possible using subpixel correlation of pre- and postseismic optical images. This technique has been successfully applied to strike-slip faulting earthquakes such as the Landers and Hector Mine events in California (Milliner *et al.*, 2016), the 2013 Balochistan earthquake in Pakistan (Vallage *et al.*, 2015), or the 2016 Kaikōura earthquake ruptures (Klinger *et al.*, 2018). Figure 6 provides an illustration of the results coming out from the same geodetic analysis (modified from Champenois, Klinger, *et al.*, 2017), clearly showing the potential for estimating the total width and amount of slip accommodated on and off the main fault. However, the process is not fully automated and subject to some judgment. For example, the calculated total slips across a given profile in Figure 6 are based on projected linear fits of the deformation field out of the fault. Selection of the appropriate linear fit can be challenging and subjective when the profiles reflect near-fault warping or tilting.

Although estimates of total deformation and fault zone width obtained from pixel-correlated stacked profiles fill a data gap that cannot be resolved with conventional field techniques, distinguishing between localized on-fault offset and distributed off-fault deformation is also of interest for engineering applications. Proportioning the total slip onto localized or mapped ruptures can be difficult and unreliable without companion field mapping or lidar analysis. For example, the secondary fault identified in profile P1 in Figure 6 is not appreciably different from other localized offsets southeast of the Kekepengu fault (e.g., at profile distance ~ 3.8 km); however, when these profiles are combined with some form of ground truthing, accurate measurements of on-fault slip, off-fault deformation, and fault zone width are obtainable.

Deriving Probabilities for FDHA

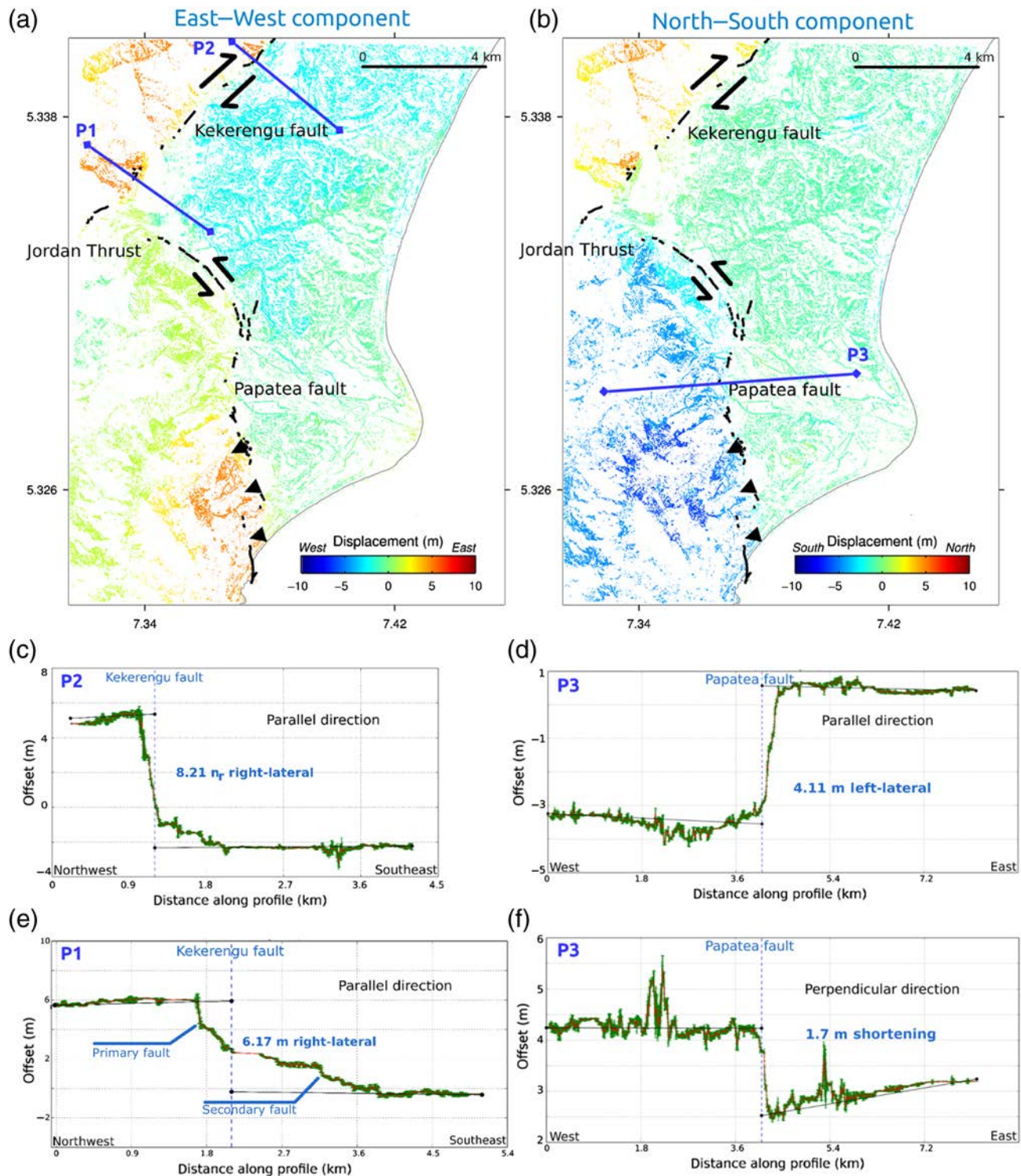
Youngs *et al.* (2003, p. 196) were the first to define “principal faulting [as] slip along the main plane (or planes) of crustal weakness responsible for the release of seismic energy during the earthquake” and “distributed faulting (...) as displacement that occurs on other faults, shears, or fractures in the vicinity of the principal rupture in response to the principal faulting,” and used this ranking to derive independent probabilities.

Based on the statement that secondary faulting is connected or structurally related to the principal rupture, we propose that the entire deformation field, including slip traces, enclosed in the coseismic crustal volume could be defined as secondary manifestation of principal slip. The volume of concern can be mapped according to InSAR, for shallow earthquakes around the world. As an example, the surface deformation related to 2010 M_w 7.2 El Mayor–Cucapah earthquake (northern Mexico) is mainly at less than 2 km around the principal fault (Fletcher *et al.*, 2014) within this strained volume imaged by the InSAR fringes (Fig. 7). However, small slip on U.S. active faults have been mapped in remote position (Rymer *et al.*, 2011; Wei, Sandwell, *et al.*, 2011; Donnellan *et al.*, 2014), and they are assigned to triggered slip probably responding to seismic waves.

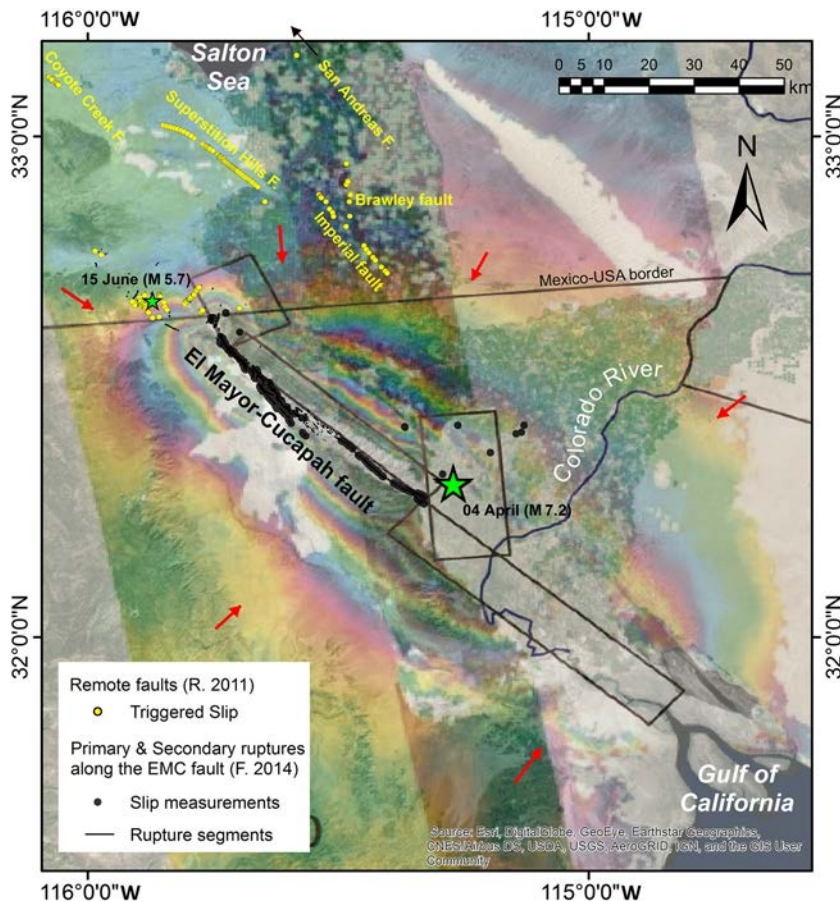
The 1992 Landers earthquake rupture produced a broad range of surface-slip amplitudes on multiple fault traces. Along the majority of the rupture, series of short ruptures with low oblique slip (maximum 30 cm) splits from a quite straight and simple trace of the South Johnson Valley or Homestead faults with dextral offsets up to 3.0 m; the former would be named distributed ruptures, the latter principal rupture. In other sections, the Landers rupture is much more complex, with multiple and overlapping continuous traces, namely the Johnson fault and the Homestead fault, which were connected by the previously unknown Kickapoo fault—but eventually recognized as a cumulative fault by Rockwell *et al.* (2000)—surrounded by distributed ruptures (Fig. 8). Dealing with the ranking, this part of the Landers surface rupture poses the issue to determine which of those three rupture(s) is (are) to be considered as primary in further statistical analyses. One solution could be to introduce an intermediary category of surface rupture, like a subsidiary principal rupture to cover the case of the large continuous rupture with significant offset mapped on a previously undescribed fault (Kickapoo segment).

Once the database historical cases are ranked in terms of principal versus distributed fault displacement, one needs to complete significant tasks before derivation of empirical relationships for PFDHA. Choosing how to estimate probability of faulting and distances is rather straightforward along primary faults. However, the same operation requires more engaging hypotheses for distributed ruptures. In the classical approach (Youngs *et al.*, 2003; Petersen *et al.*, 2011), estimation of probability occurrence of distributed faulting is performed by counting ruptured cells in a grid; then distances of distributed slip evidences are measured to a simplified principal fault trace. Another approach is used by Boncio *et al.* (2018) who measure the actual distances between principal and distributed ruptures at each secondary trace, previously discretized in a chosen interval (200 m). In this method, the distance between principal fault and distributed traces is measured perpendicular to the averaged principal fault direction. The data are used for building probability density functions, that is, the number of ruptures with respect to distance unit to the principal fault. The gridding method contains the assumption of the database completeness because counting the zero rupture pixels over the whole surface area surrounding the principal fault, whereas the method by Boncio *et al.* (2018) only considers sections of principal faults with reported distributed data to calculate the occurrence probability. The probability density functions obtained in this method can be considered as upper bounding the hazard.

An alternative to the primary versus secondary approach is to derive probabilistic displacement models based on the amplitude and spatial distribution of displacement relative to a nominal trace (Fig. 9a). Such an approach is at the very early stages of evaluation as part of the UC FDHI project (Sarmiento *et al.*, 2019). A nominal trace approach addresses the need for a linearly continuous spatial reference when developing predictive probabilistic displacement models while avoiding potentially subjective or difficult tasks of ranking of



▲ **Figure 6.** Example of application of optical correlation technique to map and measure the on-fault and near-field surface deformation during surface-rupturing earthquakes (2016 M_w 7.8 Kaikōura earthquake in New Zealand). (a,b) Horizontal displacement field from the correlation of optical images (pre-earthquake SPOT6 and postearthquake Pléiades; spatial resolution 1.8 m), using the MicMac software (see [Data and Resources](#)); coordinates are in Universal Transverse Mercator ($\times 10^5$ m for X, 10^6 m for Y). Black lines are the fault traces mapped on Pléiades images. (a) East–west component of displacement, (b) North–south component of displacement. (c–e) P1–P3 are perpendicular-to-fault profiles showing the relative displacement in parallel-to-fault (strike-slip component) direction or (f) perpendicular-to-fault (contraction or elongation) direction. Those profiles give insight on the distribution of deformation off the major fault. See [Klinger et al. \(2018\)](#) for more information on the methodology (modified from Champenois *et al.*, 2017b). The color version of this figure is available only in the electronic edition.



▲ **Figure 7.** This map superimposes the surface ruptures observed after the 2010 M_w 7+ El Mayor–Cucapah earthquake (Mexico) and a couple of Advanced Land Observation Satellites (ALOSs) ascending interferograms (15 January 2010–17 April 2010 and 17 December 2009–04 May 2010) (Wei, Fielding, *et al.*, 2011). Red arrows mark the approximate external fringe of ALOS interferograms that could match the boundary of the volume that has been strained during the 4 April M_w 7.2 earthquake. Yellow dots are the triggered-slip evidences described in Rymer *et al.* (2011) and black dots are the (primary and secondary) slip evidences by Fletcher *et al.* (2014). Green stars are the epicenters of the main event (4 April 2010) and the major aftershock to the northern tip of the fault (15 June 2010). A large part of the principal fault rupture did not reach the surface, probably accommodated in the soft-sediment pack of the Colorado River delta. Thin black rectangles represent the surface projection of the idealized fault segments used in the Wei, Fielding, *et al.* (2011) modeling to reproduce the observation datasets from seismology and geodesy. Modified from Wei, Fielding, *et al.* (2011). EMC, El Mayor–Cucapah fault. The color version of this figure is available only in the electronic edition.

mapped ruptures (e.g., primary vs. secondary) based on geological appreciation or choice. The nominal trace also provides a reference for length along rupture, a metric commonly used in displacement databases and models (e.g., Wesnousky, 2008; Petersen *et al.*, 2011), as well as a reference point for considering the sensitivity of known versus inferred rupture locations at a site.

Defining a nominal trace at the database development stage (rather than a modeling stage) has the added benefit of providing a linearly continuous spatial reference for

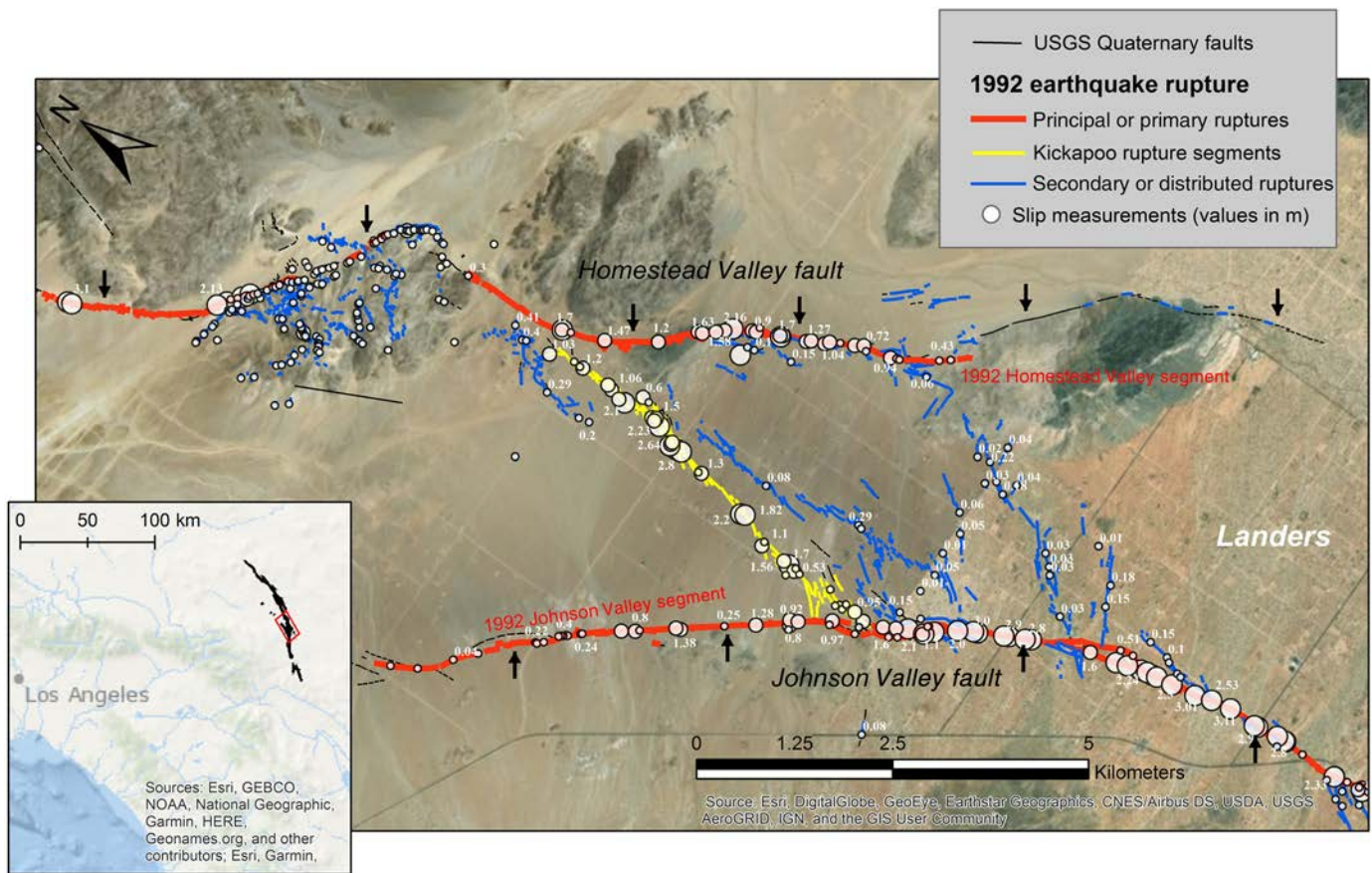
quantifying data density variability. Most earthquakes have sections of mapped ruptures that lack offset measurements (due to lack of piercing points, inaccessibility, etc.) yet surely accommodated significant displacement. This is difficult to quantify without an areal metric but nonetheless necessary for developing predictive models of fault displacements. Using a nominal trace, uniform areas or zones relative to the trace can be developed. For example, a nominal trace can be subdivided into 1 km increments, and a buffer extending 5 km on either side of the trace can define a rectangular zone (Fig. 9b). Database metrics can be cataloged by zone, such as the number of slip observations, the number of mapped ruptures, the width of mapped ruptures, and so on. Zones could also serve as the basis for fractal dimension analysis using box-counting techniques, as explored in Milliner *et al.* (2016). Collectively, these metrics can provide modelers a quantitative and objective basis for evaluating structural complexity.

SUMMARY

The PFDHA, in its earthquake approach, involve empirical relationships that need to be updated and improved. Two workshops (Paris, 2015, and Menlo Park, 2016) were focused on the construction of the SURE database for FDHA. SURE, in this first release, counts data for 45 earthquakes, with more than 15,000 slip measurements and 50,000 rupture sections. After implementation of additional literature datasets in a near future, a big challenge for the SURE database will be the enrichment in well-documented earthquakes with both geologically and geodetically derived data and the inclusion of poorly represented regions of the world (especially continental Asia and Africa).

Key long-term goals for the SURE database include incorporating the local geology information to the implemented data, adding the data derived from the aforementioned modern high-resolution techniques, and improving the global coverage of events in the database. The modern measurement techniques provide the most complete observations of surface deformation, with high-measurement density both along faults and perpendicular to faults, and these data will improve estimates of fault displacements in future earthquakes.

This first release of SURE is the proof that the mobilization of the earthquake geologists' community to fill the knowledge gaps has started. The earthquake geologists' community is encouraged to pursue the collecting, compiling, and updating of fault rupture datasets, with the effort to make them available



▲ **Figure 8.** This map shows an 18 km long section of the M_w 7.3 Landers earthquake with a complex rupture pattern, according to Petersen *et al.* (2011) dataset (original data from Hart *et al.*, 1993). Two major continuous ruptures (in red) with 1–3 m dextral offsets coincide known active faults (the Johnson and Homestead valleys faults) underlined by black arrows. In the stepover between those two strands, discontinuous and small-slip segments are considered secondary and distributed traces, whereas a rather continuous and large displacement evidences (1–3 m) connects them (the Kickapoo segment, in yellow). White labels represent the net slip values. (Inset) Location in southern California of the complete surface rupture associated with the 1992 Landers earthquake and location of the focused area. USGS, U.S. Geological Survey. The color version of this figure is available only in the electronic edition.

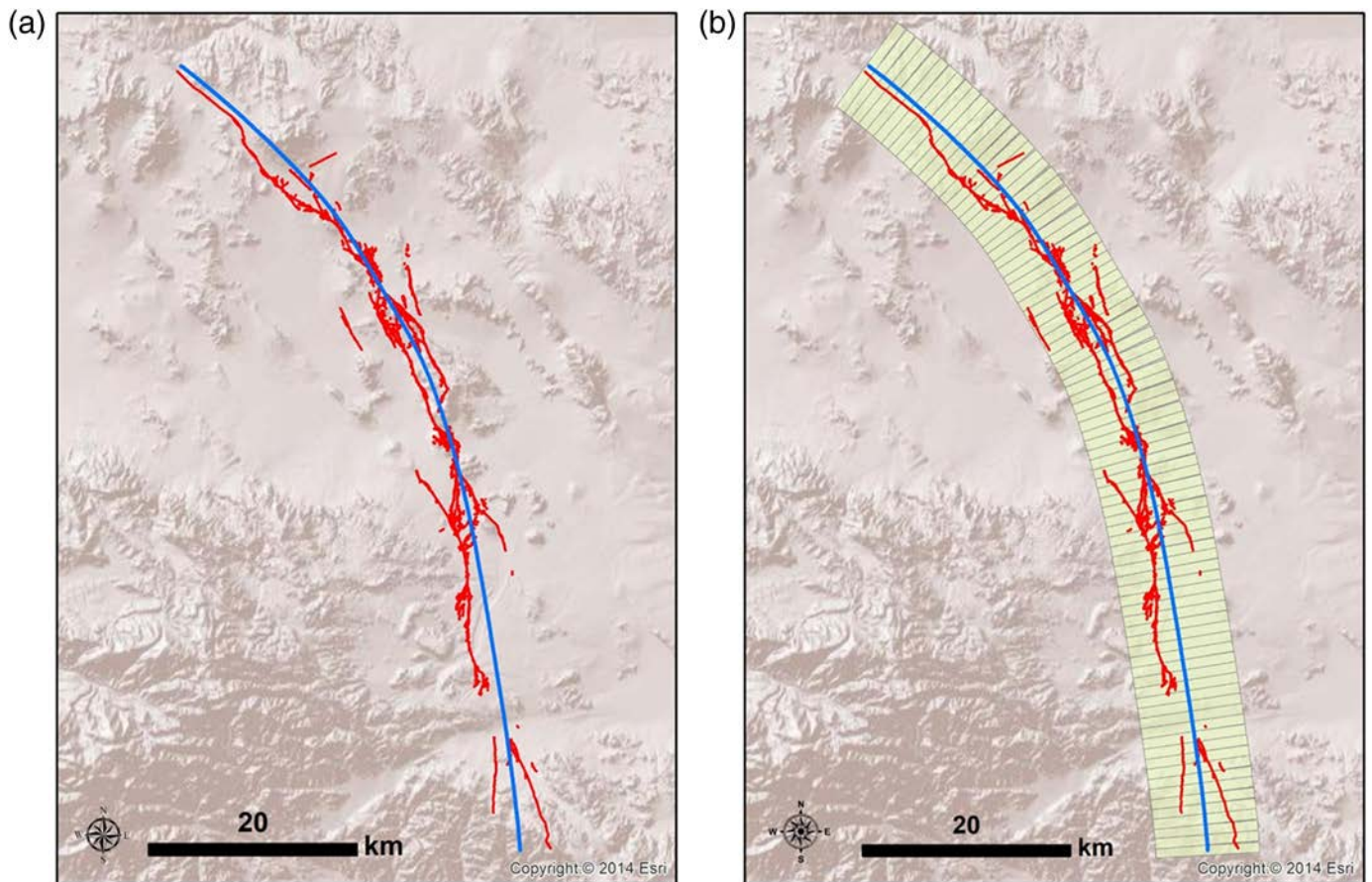
for the SURE database. The U.S. community recently initiated a multiyear study that aims to develop a database combining field and geodetic measurements of earthquake-related surface faulting to be used in surface-faulting hazard analyses in the western United States (Sarmiento *et al.*, 2019).

Populating the SURE database will provide direct benefits to the entire community for specific researches and applied sciences advances. We are opening an online exchange space and repository of data (see [Data and Resources](#)), which is guaranteed for a couple of years (European Seismological Commission).

DATA AND RESOURCES

All the data reported in the database, together with its companion article, come from published articles, documents, or maps. In the © supplemental content, we report data and

models from the U.S. Geological Survey (USGS) fault database (<https://earthquake.usgs.gov/hazards/qfaults/>), from the GNS active faults database (<http://data.gns.cri.nz/af/>), the International Seismological Centre-Global Earthquake Model (ISC-GEM) earthquake database (ISC-GEM Earthquake Catalogue, 2019, doi: [10.31905/D808B825](https://doi.org/10.31905/D808B825)), from the SRCMOD online database of slip distributions (<http://equake-rc.info/SRCMOD/>), and from the CRUST 1.0 model for crustal thickness (<https://igppweb.ucsd.edu/~gabi/crust1.html>). The information about Trans-Alaska oil pipeline is available at <https://pubs.usgs.gov/fs/2003/fs014-03/pipeline.html>. The Fault2SHA European Seismological Commission (ESC) working group is available at www.fault2sha.net. MicMac software is available at <https://micmac.engg.eu/index.php/Accueil>. The USGS earthquake hazards program website is available at <https://earthquake.usgs.gov/earthquakes/>. All websites were last accessed on June 2019. ☒



▲ **Figure 9.** Example definition of nominal trace and zones for 1992 Landers earthquake. (a,b) Red lines are field mapped ruptures from USGS Quaternary Fault and Fold Database. Blue line is nominal trace. (b) Light green rectangles are zones 1 km long and 10 km wide. The color version of this figure is available only in the electronic edition.

ACKNOWLEDGMENTS

Institut de Radioprotection et de Sûreté Nucléaire (IRSN) organized and funded the first meeting in October 2015 in Paris, France, with 20 attendees from New Zealand, South America, United States, Italy, United Kingdom, and France. The U.S. Geological Survey (USGS) and California Geological Survey (CGS) were in charge of funding and organizing the second workshop in Menlo Park (U.S.A.), in December 2016. More than 110 scientists, stakeholders, and engineers attended. The authors are grateful to those who contributed to the initial discussions, especially Yoshi Fukushima (International Atomic Energy Agency [IAEA], Vienna, Austria), Christophe Clément, Hervé Jomard, and Marc Cushing (IRSN, France), Yann Klinger (Institut du Physique du Globe de Paris [IPGP]), Thomas Chartier (Ecole Normale Supérieure Paris [ENS], France), Eugénie Pérouse (Centre Européen de Recherche et d'Enseignement des Géosciences de l'Environnement [CEREGE], France), Jochen Hürtgen (University of Aachen, Germany), Austin Elliott and Richard Walker (Centre for the Observation and Modelling of Earthquakes, Volcanoes and Tectonics [COMET], United Kingdom), and Alessandro Maria Michetti (University of Como, Italy). The authors also

give credit to Christopher Milliner (reviewer) and to Zhigang Peng (Editor-in-Chief) who promptly and efficiently helped us improve our work. The SURface Ruptures due to Earthquakes (SURE) initiative is part of the SURFACE project supported by the International Union for Quaternary Research (INQUA; www.earthquakegeology.com, last accessed July 2019) between 2016 and 2019. It is linked to the IAEA effort to formalize the Fault Displacement Hazard Analysis (FDHA) into a pending Technical Document (TECDOC) to which some of the authors are contributors.

All six first authors contributed equally to this work (writing, data compilation); the other authors were classified by alphabetical order.

REFERENCES

- Arrowsmith, J. R., C. J. Crosby, A. M. Korzhonkov, E. Mamyrov, I. Povolotskaya, B. Guralnik, and A. Landgraf (2017). Surface rupture of the 1911 Kebin (Chon-Kemin) earthquake, Northern Tien Shan, Kyrgyzstan, *Geol. Soc. Lond. Spec. Publ.* **432**, 233–253, doi: [10.1144/SP432.10](https://doi.org/10.1144/SP432.10).
- Baize, S., and O. Scotti (2017). *Fault Displacement Hazard Analysis Workshop in Menlo Park (USGS, California) - 8-9/12/2016 -*

- Synthesis and Perspectives*, Institut Radioprotection Sûreté Nucléaire, doi: [10.5281/zenodo.1041821](https://doi.org/10.5281/zenodo.1041821).
- Baize, S., F. Cinti, C. Costa, T. Dawson, A. Elliott, L. Guerrieri, J. McCalpin, K. Okumura, O. Scotti, M. Takao, *et al.* (2016). *Surface Rupture Database for Seismic Hazard Assessment - 2015 Report of the Kick-Off Meeting of the SURE Database Working Group*, Institut Radioprotection Sûreté Nucléaire, doi: [10.5281/zenodo.2314963](https://doi.org/10.5281/zenodo.2314963).
- Barka, A., H. S. Akyüz, E. Altunel, G. Sunal, Z. Çakir, A. Dikbas, B. Yerli, R. Armijo, B. Meyer, J. B. Chabaliere, *et al.* (2002). The surface rupture and slip distribution of the 17 August 1999 İzmit earthquake (M 7.4), North Anatolian Fault, *Bull. Seismol. Soc. Am.* **92**, 43–60, doi: [10.1785/0120000841](https://doi.org/10.1785/0120000841).
- Beanland, S., and M. M. Clark (1994). The Owens Valley fault zone, eastern California, and surface faulting associated with the 1872 earthquake, *U.S. Geol. Surv. Bull.* No. 1982, doi: [10.3133/b1982](https://doi.org/10.3133/b1982).
- Beanland, S., K. R. Berryman, and G. H. Blick (1989). Geological investigations of the 1987 Edgecumbe earthquake, New Zealand, *New Zeal. J. Geol. Geophys.* **32**, 73–91, doi: [10.1080/00288306.1989.10421390](https://doi.org/10.1080/00288306.1989.10421390).
- Boncio, P., F. Liberi, M. Caldarella, and F.-C. Nurminen (2018). Width of surface rupture zone for thrust earthquakes: Implications for earthquake fault zoning, *Nat. Hazards Earth Syst. Sci.* **18**, 241–256, doi: [10.5194/nhess-18-241-2018](https://doi.org/10.5194/nhess-18-241-2018).
- Bonilla, M. G., J. M. Buchanan, R. O. Castle, M. M. Clark, V. A. Frizzell, R. M. Gulliver, F. K. Miller, J. P. Pinkerton, D. C. Ross, R. V. Sharp, *et al.* (1971). The San Fernando, California, earthquake of February 9, 1971. *U.S. Geol. Surv. Prof. Pap.* **733**, 55–76.
- Brozzetti, F., P. Boncio, D. Cirillo, F. Ferrarini, R. Nardis, A. Testa, F. Liberi, and G. Lavecchia (2019). High-resolution field mapping and analysis of the August–October 2016 coseismic surface faulting (Central Italy earthquakes): Slip distribution, parameterization, and comparison with global earthquakes, *Tectonics* **38**, 417–439, doi: [10.1029/2018TC005305](https://doi.org/10.1029/2018TC005305).
- Caskey, S. J., S. G. Wesnousky, P. Zhang, and D. B. Slemmons (1996). Surface faulting of the 1954 Fairview Peak (MS 7.2) and Dixie Valley (MS 6.8) earthquakes, central Nevada, *Bull. Seismol. Soc. Am.* **86**, 761–787.
- Castellanos, A. (1944). Contribución a los estudios sísmicos en la República Argentina, in *El caso de San Juan (1944) (No. I, II, III)*, Monografías, Universidad Nacional del Litoral, Rosario, Argentina.
- Champanois, J., S. Baize, M. Vaille, H. Jomard, A. Alvarado, P. Espin, G. Ekstöm, and L. Audin (2017). Evidences of surface rupture associated with a low-magnitude (Mw 5.0) shallow earthquake in the Ecuadorian Andes: Andean earthquake surface rupture, *J. Geophys. Res.* **122**, 8446–8458, doi: [10.1002/2017JB013928](https://doi.org/10.1002/2017JB013928).
- Champanois, J., Y. Klinger, R. Grandin, C. Satriano, S. Baize, A. Delorme, and O. Scotti (2017). Surface rupture and slip distribution of the 2016 Mw7.8 Kaikoura earthquake (New Zealand) from optical satellite image correlation using MicMac, presented at the *SSA 2017 Annual Meeting*, Denver, Colorado, 18–20 April 2017, 655 pp.
- Chen, R., and M. D. Petersen (2011). Probabilistic fault displacement hazards for the southern San Andreas fault using scenarios and empirical slips, *Earthq. Spectra* **27**, 293–313, doi: [10.1193/1.3574226](https://doi.org/10.1193/1.3574226).
- Choi, J.-H., Y. Klinger, M. Ferry, J.-F. Ritz, R. Kurtz, M. Rizza, L. Bollinger, B. Davaasambuu, N. Tsend-Ayush, and S. Demberel (2018). Geologic inheritance and earthquake rupture processes: The 1905 M ≥ 8 Tsetserleg-Bulnay strike-slip earthquake sequence, Mongolia, *J. Geophys. Res.* **123**, 1925–1953, doi: [10.1002/2017JB013962](https://doi.org/10.1002/2017JB013962).
- Cinti, F. R., R. Civico, A. M. Blumetti, L. Guerrieri, and G. Leoni (2018). INGV - ISPRA joint surface faulting database - Mw 6.1, 2009, April 6th L'Aquila earthquake (Central Italy), *PANGAEA* doi: [10.1594/PANGAEA.889132](https://doi.org/10.1594/PANGAEA.889132).
- Cinti, F. R., D. Pantosti, P. M. De Martini, S. Pucci, R. Civico, S. Pierdominici, L. Cucci, C. A. Brunori, S. Pinzi, and A. Patera (2011). Evidence for surface faulting events along the Paganica fault prior to the 6 April 2009 L'Aquila earthquake (central Italy), *J. Geophys. Res.* **116**, doi: [10.1029/2010JB007988](https://doi.org/10.1029/2010JB007988).
- Civico, R., S. Pucci, F. Villani, L. Pizzimenti, P. M. De Martini, R. Nappi, and the Open EMERGEIO Working Group (2018). Surface ruptures following the 30 October 2016 Mw 6.5 Norcia earthquake, central Italy, *J. Maps* **14**, 151–160, doi: [10.1080/17445647.2018.1441756](https://doi.org/10.1080/17445647.2018.1441756).
- Clark, M. M. (1972). Surface rupture along the Coyote Creek fault, in *The Borrego Mountain Earthquake of April 9, 1968*, Geol. Surv. Prof. Pap., U.S. Department of the Interior, Washington, D.C., 55–86.
- Clark, M. M., J. C. Yount, P. R. Vaughn, and R. L. Zepeda, (1982). Map showing surface ruptures associated with the Mammoth Lakes, California, earthquakes of May 1980, *Misc. Field Stud. Map 1396*, doi: [10.3133/mf1396](https://doi.org/10.3133/mf1396).
- Crone, A. J., M. N. Machette, M. G. Bonilla, J. J. Lienkaemper, K. L. Pierce, W. E. Scott, and R. C. Bucknam (1987). Surface faulting accompanying the Borah Peak earthquake and segmentation of the lost river fault, central Idaho, *Bull. Seismol. Soc. Am.* **77**, 739–770.
- DeLong, S. B., A. Donnellan, D. J. Ponti, R. S. Rubin, J. J. Lienkaemper, C. S. Prentice, T. E. Dawson, G. Seitz, D. P. Schwartz, K. W. Hudnut, *et al.* (2016). Tearing the terroir: Details and implications of surface rupture and deformation from the 24 August 2014 M 6.0 South Napa earthquake, California, *Earth Space Sci.* **3**, 416–430, doi: [10.1002/2016EA000176](https://doi.org/10.1002/2016EA000176).
- Donnellan, A., J. Parker, S. Hensley, M. Pierce, J. Wang, and J. Rundle (2014). UAVSAR observations of triggered slip on the Imperial, Superstition Hills, and East Elmore Ranch faults associated with the 2010 M 7.2 El Mayor-Cucapah earthquake, *Geochem. Geophys. Geosys.* **15**, 815–829, doi: [10.1002/2013GC005120](https://doi.org/10.1002/2013GC005120).
- Fletcher, J. M., O. J. Teran, T. K. Rockwell, M. E. Oskin, K. W. Hudnut, K. J. Mueller, R. M. Spelz, S. O. Akciz, E. Masana, G. Faneros, *et al.* (2014). Assembly of a large earthquake from a complex fault system: Surface rupture kinematics of the 4 April 2010 El Mayor–Cucapah (Mexico) Mw 7.2 earthquake, *Geosphere* **10**, 797–827, doi: [10.1130/GES00933.1](https://doi.org/10.1130/GES00933.1).
- Gold, P. O., M. E. Oskin, A. J. Elliott, A. Hinojosa-Corona, M. H. Taylor, O. Kreylos, and E. Cowgill (2013). Coseismic slip variation assessed from terrestrial lidar scans of the El Mayor–Cucapah surface rupture, *Earth Planet. Sci. Lett.* **366**, 151–162, doi: [10.1016/j.epsl.2013.01.040](https://doi.org/10.1016/j.epsl.2013.01.040).
- Haeussler, P. J., D. P. Schwartz, T. E. Dawson, H. D. Stenner, J. J. Lienkaemper, B. Sherrod, F. R. Cinti, P. Montone, P. A. Craw, A. J. Crone, and S. F. Personius (2004). Surface rupture and slip distribution of the Denali and Totschunda faults in the 3 November 2002 M 7.9 earthquake, Alaska, *Bull. Seismol. Soc. Am.* **94**, S23–S52, doi: [10.1785/0120040626](https://doi.org/10.1785/0120040626).
- Hanks, T. C., and H. Kanamori (1979). A moment magnitude scale, *J. Geophys. Res.* **84**, 2348, doi: [10.1029/JB084iB05p02348](https://doi.org/10.1029/JB084iB05p02348).
- Hart, E. W., W. A. Bryant, and J. A. Treiman (1993). Surface faulting associated with the June 1992 Landers earthquake, California, *Calif. Geol.* **46**, 10–16.
- Hartleb, R. D., J. F. Dolan, H. S. Akyüz, T. E. Dawson, A. Z. Tucker, B. Yerli, T. K. Rockwell, E. Toraman, Z. Çakir, A. Dikbaş, and E. Altunel (2002). Surface rupture and slip distribution along the Karadere segment of the 17 August 1999 İzmit and the western section of the 12 November 1999 Düzce, Turkey, earthquakes, *Bull. Seismol. Soc. Am.* **92**, 67–78, doi: [10.1785/0120000829](https://doi.org/10.1785/0120000829).
- Hemphill-Haley, M. A., and R. J. Weldon (1999). Estimating prehistoric earthquake magnitude from point measurements of surface rupture, *Bull. Seismol. Soc. Am.* **89**, 1264–1279.
- Inbal, A., J.-P. Ampuero, and J.-P. Avouac (2017). Locally and remotely triggered aseismic slip on the central San Jacinto Fault near Anza, CA, from joint inversion of seismicity and strainmeter data, *J. Geophys. Res.* **122**, 3033–3061, doi: [10.1002/2016JB013499](https://doi.org/10.1002/2016JB013499).
- International Seismological Centre-Global Earthquake Model (ISC-GEM) Earthquake Catalogue (2019). *ISC-GEM Global Instrumental Earthquake Catalogue*, Version 6.0, doi: [10.31905/D808B825](https://doi.org/10.31905/D808B825).

- Jennings, P. C. (1997). Enduring lessons and opportunities lost from the San Fernando earthquake of February 9, 1971, *Earthq. Spectra* **13**, 25–44, doi: [10.1193/1.1585930](https://doi.org/10.1193/1.1585930).
- Kamb, B., L. T. Silver, M. J. Abrams, B. A. Carter, H. Jordan, and J. B. Minster (1971). Pattern of faulting and nature of fault movement in the San Fernando earthquake, *U.S. Geol. Surv. Profess. Pap.* **733**, 41–75.
- Katsube, A., H. Kondo, K. Taniguchi, and Y. Kase (2017). Surface rupture and slip associated with the 2014 Nagano-ken Hokubu earthquake (Mw 6.2), *J. Geol. Soc. Japan* **123**, 1–21, doi: [10.5575/geosoc.2016.0048](https://doi.org/10.5575/geosoc.2016.0048).
- Kearse, J., T. A. Little, R. J. V. Dissen, P. M. Barnes, R. Langridge, J. Mountjoy, W. Ries, P. Villamor, K. J. Clark, A. Benson, *et al.* (2018). Onshore to offshore ground-surface and seabed rupture of the Jordan–Kekerengu–Needles fault network during the 2016 Mw 7.8 Kaikōura earthquake, New Zealand, *Bull. Seismol. Soc. Am.* **108**, 1573–1595, doi: [10.1785/0120170304](https://doi.org/10.1785/0120170304).
- Klinger, Y., K. Okubo, A. Vallage, J. Champenois, A. Delorme, E. Rougier, Z. Lei, E. E. Knight, A. Munjiza, C. Satriano, *et al.* (2018). Earthquake damage patterns resolve complex rupture processes, *Geophys. Res. Lett.* **45**, 10,279–10,287, doi: [10.1029/2018GL078842](https://doi.org/10.1029/2018GL078842).
- Kurtz, R., Y. Klinger, M. Ferry, and J.-F. Ritz (2018). Horizontal surface-slip distribution through several seismic cycles: The eastern Bogd fault, Gobi-Altai, Mongolia, *Tectonophysics* **734/735**, 167–182, doi: [10.1016/j.tecto.2018.03.011](https://doi.org/10.1016/j.tecto.2018.03.011).
- Langridge, R. M., J. Rowland, P. Villamor, J. Mountjoy, D. B. Townsend, E. Nissen, C. Madugo, W. F. Ries, C. Gasston, A. Canva, *et al.* (2018). Coseismic rupture and preliminary slip estimates for the Papatea fault and its role in the 2016 Mw 7.8 Kaikōura, New Zealand, earthquake, *Bull. Seismol. Soc. Am.* **108**, 1596–1622, doi: [10.1785/0120170336](https://doi.org/10.1785/0120170336).
- Langridge, R. M., H. D. Stenner, T. E. Fumal, S. A. Christofferson, T. K. Rockwell, R. D. Hartleb, J. Bachhuber, and A. A. Barka (2002). Geometry, slip distribution, and kinematics of surface rupture on the Sakarya fault segment during the 17 August 1999 İzmit, Turkey, earthquake, *Bull. Seismol. Soc. Am.* **92**, 107–125, doi: [10.1785/0120000804](https://doi.org/10.1785/0120000804).
- Lettis, W. R., D. L. Wells, and J. N. Baldwin (1997). Empirical observations regarding reverse earthquakes, blind thrust faults, and quaternary deformation: Are blind thrust faults truly blind?, *Bull. Seismol. Soc. Am.* **87**, 1171–1198.
- Litchfield, N. J., R. J. Van Dissen, S. Hornblow, M. Quigley, and G. C. Archibald (2014). Detailed analysis of Greendale Fault ground surface rupture displacements and geometries, *GNS Sci. Rept. 2013/18*, available at http://shop.gns.cri.nz/sr_2013-018-pdf/ (last accessed April 2019).
- Litchfield, N. J., P. Villamor, R. J. V. Dissen, A. Nicol, P. M. Barnes, D. J. A. Barrell, J. R. Pettinga, R. M. Langridge, T. A. Little, J. J. Mountjoy, *et al.* (2018). Surface rupture of multiple crustal faults in the 2016 Mw 7.8 Kaikōura, New Zealand, earthquake, *Bull. Seismol. Soc. Am.* **108**, 1496–1520, doi: [10.1785/0120170300](https://doi.org/10.1785/0120170300).
- Mai, P. M., and K. K. S. Thingbaijam (2014). SRCMOD: An online database of finite-fault rupture models, *Seismol. Res. Lett.* **85**, 1348–1357, doi: [10.1785/0220140077](https://doi.org/10.1785/0220140077).
- Milliner, C. W. D., C. Sammis, A. A. Allam, J. F. Dolan, J. Hollingsworth, S. Leprince, and F. Ayoub (2016). Resolving fine-scale heterogeneity of co-seismic slip and the relation to fault structure, *Sci. Rep.* **6**, doi: [10.1038/srep27201](https://doi.org/10.1038/srep27201).
- Moss, R. E. S., and Z. E. Ross (2011). Probabilistic fault displacement hazard analysis for reverse faults, *Bull. Seismol. Soc. Am.* **101**, 1542–1553, doi: [10.1785/0120100248](https://doi.org/10.1785/0120100248).
- Moss, R. E. S., M. Buelna, and K. V. Stanton (2018). Physical, analytical, and numerical modeling of reverse-fault displacement through near-surface soils, *Bull. Seismol. Soc. Am.* **108**, 3149–3159, doi: [10.1785/0120180067](https://doi.org/10.1785/0120180067).
- Myers, W. B., and W. Hamilton (1964). Deformation accompanying the Hebgen Lake earthquake of August 17, 1959, in *The Hebgen Lake, Montana Earthquake of August 17, 1959*, Geol. Surv. Profess. Pap. U.S. Department of the Interior, Washington, D.C., 55–98.
- Nicol, A., N. Khajavi, J. R. Pettinga, C. Fenton, T. Stahl, S. Bannister, K. Pedley, N. Hyland-Brook, T. Bushell, I. Hamling, *et al.* (2018). Preliminary geometry, displacement, and kinematics of fault ruptures in the epicentral region of the 2016 Mw 7.8 Kaikōura, New Zealand, earthquake, *Bull. Seismol. Soc. Am.* **108**, 1521–1539, doi: [10.1785/0120170329](https://doi.org/10.1785/0120170329).
- Oettle, N. K., and J. D. Bray (2013). Geotechnical mitigation strategies for earthquake surface fault rupture, *J. Geotech. Geoenviron. Eng.* **139**, 1864–1874, doi: [10.1061/\(ASCE\)GT.1943-5606.0000933](https://doi.org/10.1061/(ASCE)GT.1943-5606.0000933).
- Okumura, K. (2001). Paleoseismology of the Itoigawa-Shizuoka tectonic line in central Japan, *J. Seismol.* **5**, 411–431, doi: [10.1023/A:1011483811145](https://doi.org/10.1023/A:1011483811145).
- Petersen, M. D., T. E. Dawson, R. Chen, T. Cao, C. J. Wills, D. P. Schwartz, and A. D. Frankel (2011). Fault displacement hazard for strike-slip faults, *Bull. Seismol. Soc. Am.* **101**, 805–825, doi: [10.1785/0120100035](https://doi.org/10.1785/0120100035).
- Pezzopane, S. K., and T. E. Dawson (1996). Seismotectonic framework and characterization of faulting at Yucca Mountain, Nevada, *Chapter 9: Fault Displacement Hazard: A Summary Of Issues And Information*, U.S. Geol. Surv. Admin. Rep. for U.S. Department of Energy.
- Philip, H., and M. Meghraoui (1983). Structural analysis and interpretation of the surface deformations of the El Asnam earthquake of October 10, 1980, *Tectonics* **2**, 17–49, doi: [10.1029/TC002i001p00017](https://doi.org/10.1029/TC002i001p00017).
- Ponti, D. J., C. M. Rosa, and J. L. Blair (2019). The Mw 6.0 South Napa earthquake of August 24, 2014—Observations of surface faulting and ground deformation, with recommendations for improving post-earthquake field investigations, *U.S. Geol. Surv. Open-File Rept. 2019-1018*, 50 pp. + 15 appendices, available at <https://pubs.usgs.gov/of/2019/1018/> (last accessed March 2019).
- Quigley, M., R. Van Dissen, N. Litchfield, P. Villamor, B. Duffy, D. Barrell, K. Furlong, T. Stahl, E. Bilderback, and D. Noble (2012). Surface rupture during the 2010 Mw 7.1 Darfield (Canterbury) earthquake: Implications for fault rupture dynamics and seismic-hazard analysis, *Geology* **40**, 55–58, doi: [10.1130/G32528.1](https://doi.org/10.1130/G32528.1).
- Rockwell, T. K., S. Lindvall, M. Herzberg, D. Murbach, T. Dawson, and G. Berger (2000). Paleoseismology of the Johnson Valley, Kickapoo, and Homestead Valley Faults: Clustering of earthquakes in the eastern California shear zone, *Bull. Seismol. Soc. Am.* **90**, 1200–1236, doi: [10.1785/0119990023](https://doi.org/10.1785/0119990023).
- Rymer, M. J., J. A. Treiman, K. J. Kendrick, J. J. Lienkaemper, R. J. Weldon, R. Bilham, M. Wei, E. J. Fielding, J. L. Hernandez, B. P. E. Olson *et al.* (2011). Triggered surface slips in southern California associated with the 2010 El Mayor-Cucapah, Baja California, Mexico, earthquake, *Open-File Rept. 2010-1333*, Reston, Virginia, 62 pp., available at <https://pubs.usgs.gov/of/2010/1333/> (last accessed May 2017).
- Sarmiento, A., N. Abrahamson, S. Baize, Y. Bozorgnia, R. Chen, K. Coppersmith, T. E. Dawson, J. L. Donahue, V. Jacob, M. Ketabdar, *et al.* (2019). A new model database for next-generation fault displacement hazard analysis, presented at the *SSA Annual Meeting*, Seattle, Washington, 23–26 April 2019.
- Schwartz, D. P., J. J. Lienkaemper, S. Hecker, K. I. Kelson, T. E. Fumal, J. N. Baldwin, G. G. Seitz, and T. M. Niemi (2014). The earthquake cycle in the San Francisco Bay Region: A.D. 1600–2012, *Bull. Seismol. Soc. Am.* **104**, 1299–1328, doi: [10.1785/0120120322](https://doi.org/10.1785/0120120322).
- Sharp, R. V., K. E. Budding, J. Boatwright, M. J. Ader, M. G. Bonilla, M. M. Clark, T. E. Fumal, K. K. Harms, J. J. Lienkaemper, D. M. Morton, *et al.* (1989). Surface faulting along the Superstition Hills fault zone and nearby faults associated with the earthquakes of 24 November 1987, *Bull. Seismol. Soc. Am.* **79**, 252–281.
- Sharp, R. V., J. J. Lienkaemper, M. G. Bonilla, D. B. Burke, B. F. Fox, D. G. Herd, D. M. Miller, D. M. Morton, D. J. Ponti, M. J. Rymer, *et al.* (1982). Surface faulting in the central Imperial Valley, in *The*

- Imperial Valley, California, Earthquake of October 15, 1979*, Geol. Surv. Profess. Pap., U.S. Department of the Interior, Washington, D.C., 119–144.
- Shirahama, Y., M. Yoshimi, Y. Awata, T. Maruyama, T. Azuma, Y. Miyashita, H. Mori, K. Imanishi, N. Takeda, T. Ochi, *et al.* (2016). Characteristics of the surface ruptures associated with the 2016 Kumamoto earthquake sequence, central Kyushu, Japan, *Earth Planets Space* **68**, doi: [10.1186/s40623-016-0559-1](https://doi.org/10.1186/s40623-016-0559-1).
- Stanton, K. (2013). Investigation of parameters influencing reverse fault rupture propagation to the ground surface, *M.S. Thesis*, Faculty of California Polytechnic State University, San Luis Obispo, California.
- Suter, M. (2015). Rupture of the Pitáycachi Fault in the 1887 Mw 7.5 Sonora, Mexico earthquake (southern Basin-and-Range Province): Rupture kinematics and epicenter inferred from rupture branching patterns, *J. Geophys. Res.* **120**, 617–641, doi: [10.1002/2014JB011244](https://doi.org/10.1002/2014JB011244).
- Takao, M., J. Tsuchiyama, T. Annaka, and T. Kurita (2013). Application of probabilistic fault displacement hazard analysis in Japan, *J. Japan Assoc. Earthq. Eng.* **13**, 17–36, doi: [10.5610/jaee.13.17](https://doi.org/10.5610/jaee.13.17).
- Teran, O. J., J. M. Fletcher, M. E. Oskin, T. K. Rockwell, K. W. Hudnut, R. M. Spelz, S. O. Akciz, A. P. Hernandez-Flores, and A. E. Morelan (2015). Geologic and structural controls on rupture zone fabric: A field-based study of the 2010 Mw 7.2 El Mayor-Cucapah earthquake surface rupture, *Geosphere* **11**, 899–920, doi: [10.1130/GES01078.1](https://doi.org/10.1130/GES01078.1).
- Treiman, J. A., K. J. Kendrick, W. A. Bryant, T. K. Rockwell, and S. F. McGill (2002). Primary surface rupture associated with the Mw 7.1 16 October 1999 Hector Mine earthquake, San Bernardino County, California, *Bull. Seismol. Soc. Am.* **92**, 1171–1191, doi: [10.1785/0120000923](https://doi.org/10.1785/0120000923).
- Vallage, A., Y. Klinger, R. Grandin, H. S. Bhat, and M. Pierrot-Deseilligny (2015). Inelastic surface deformation during the 2013 Mw 7.7 Balochistan, Pakistan, earthquake, *Geology* **43**, 1079–1082, doi: [10.1130/G37290.1](https://doi.org/10.1130/G37290.1).
- Victor, P., O. Oncken, M. Sobiesiak, M. Kemter, G. Gonzalez, and T. Ziegenhagen (2018). Dynamic triggering of shallow slip on forearc faults constrained by monitoring surface displacement with the IPOC Creepmeter Array, *Earth Planet. Sci. Lett.* **502**, 57–73, doi: [10.1016/j.epsl.2018.08.046](https://doi.org/10.1016/j.epsl.2018.08.046).
- Villamor, P., N. Litchfield, D. Barrell, R. Van Dissen, S. Hornblow, M. Quigley, S. Levick, W. Ries, B. Duffy, J. Begg, *et al.* (2012). Map of the 2010 Greendale Fault surface rupture, Canterbury, New Zealand: Application to land use planning, *New Zeal. J. Geol. Geophys.* **55**, 223–230, doi: [10.1080/00288306.2012.680473](https://doi.org/10.1080/00288306.2012.680473).
- Villani, F., R. Civico, S. Pucci, L. Pizzimenti, R. Nappi, P. M. De Martini, and the Open EMERGE Working Group (2018). A database of the coseismic effects following the 30 October 2016 Norcia earthquake in Central Italy, *Sci. Data* **5**, 180049, doi: [10.1038/sdata.2018.49](https://doi.org/10.1038/sdata.2018.49).
- Wallace, R. E. (1984). Fault scarps formed during the earthquakes of October 2, 1915, in Pleasant Valley, Nevada, and some tectonic implications, in *Faulting Related to the 1915 Earthquakes in the Pleasant Valley, Nevada*, U.S. Geol. Surv. Profess. Pap., Washington, D.C., 1–33.
- Wei, M., D. Sandwell, Y. Fialko, and R. Bilham (2011). Slip on faults in the Imperial Valley triggered by the 4 April 2010 Mw 7.2 El Mayor-Cucapah earthquake revealed by InSAR, *Geophys. Res. Lett.* **38**, doi: [10.1029/2010GL045235](https://doi.org/10.1029/2010GL045235).
- Wei, S., E. Fielding, S. Leprince, A. Sladen, J.-P. Avouac, D. Helmberger, E. Hauksson, R. Chu, M. Simons, K. Hudnut, *et al.* (2011). Superficial simplicity of the 2010 El Mayor-Cucapah earthquake of Baja California in Mexico, *Nat. Geosci.* **4**, 615–618, doi: [10.1038/ngeo1213](https://doi.org/10.1038/ngeo1213).
- Wells, D. L., and K. J. Coppersmith (1994). New empirical relationships among magnitude, rupture length, rupture width, rupture area, and surface displacement, *Bull. Seismol. Soc. Am.* **84**, 974–1002.
- Wesnousky, S. G. (2008). Displacement and geometrical characteristics of earthquake surface ruptures: Issues and implications for seismic hazard analysis and the process of earthquake rupture, *Bull. Seismol. Soc. Am.* **98**, 1609–1632, doi: [10.1785/0120070111](https://doi.org/10.1785/0120070111).
- Williams, J. N., D. J. A. Barrell, M. W. Stirling, K. M. Sauer, G. C. Duke, and K. X. Hao (2018). Surface rupture of the Hundalee fault during the 2016 Mw 7.8 Kaikōura earthquake, *Bull. Seismol. Soc. Am.* **108**, 1540–1555, doi: [10.1785/0120170291](https://doi.org/10.1785/0120170291).
- Youngs, R. R., W. J. Arabasz, R. E. Anderson, A. R. Ramelli, J. P. Ake, D. B. Slemmons, J. P. McCalpin, D. I. Doser, C. J. Fridrich, F. H. Swan, *et al.* (2003). A methodology for probabilistic fault displacement hazard analysis (PFDHA), *Earthq. Spectra* **19**, 191–219, doi: [10.1193/1.1542891](https://doi.org/10.1193/1.1542891).
- Yu, G., X. Xu, Y. Klinger, G. Diao, G. Chen, X. Feng, C. Li, A. Zhu, R. Yuan, T. Guo, *et al.* (2010). Fault-scarp features and cascading-rupture model for the M_w 7.9 Wenchuan earthquake, Eastern Tibetan Plateau, China, *Bull. Seismol. Soc. Am.* **100**, 2590–2614, doi: [10.1785/0120090255](https://doi.org/10.1785/0120090255).

Stéphane Baize

Oona Scotti

PSE-ENV Seismic Hazard Division

Institut de Radioprotection et Sûreté Nucléaire

Rue de la Redoute

92260 Fontenay-aux-Roses

France

stephane.baize@irsn.fr

oona.scotti@irsn.fr

Fiiia Nurminen

Paolo Boncio

Dipartimento DiSPuTer

Universita' G. d'Annunzio di Chieti-Pescara

Via dei Vestini 31

66100 Chieti Scalo, Italy

fiiia.nurminen@unich.it

paolo.boncio@unich.it

Alexandra Sarmiento

The B. John Garrick Institute for the Risk Sciences

University of California Los Angeles (UCLA)

Engineering VI 5th Floor

404 Westwood Plaza

Los Angeles, California 90095 U.S.A.

asarmy@ucla.edu

Timothy Dawson

California Geological Survey

1900 South Norfolk Street, Suite 300

San Mateo, California 94403 U.S.A.

Timothy.Dawson@conservation.ca.gov

Makoto Takao

Civil and Architectural Engineering Management Office,

Engineering Strategy Unit

Tokyo Electric Power Company (TEPCO) Holdings, Inc.

1-1-3 Uchisaiwai-cho, Chiyoda-ku

Tokyo 100-8560, Japan

takaom@atena-j.jp

Takashi Azuma
Research Institute of Earthquake & Volcano Geology
National Institute of Advanced Industrial Science and
Technology
Site Central 7, 1-1-1, Higashi
Tsukuba 3058567, Japan
t-azuma@aist.go.jp

Johann Champenois
Etienne Marti¹
Laboratoire de Tectonique et Mécanique de la Lithosphère
Institut de Physique du Globe de Paris
1 Rue Jussieu, 75005 Paris
France
titchampos@hotmail.com
etienne.marti@outlook.fr

Francesca R. Cinti
Riccardo Civico
Istituto Nazionale Geofisica Vulcanologia
Sezione Roma 1
Via di Vigna Murata 605
00143 Rome, Italy
francesca.cinti@ingv.it
riccardo.civico@ingv.it

Carlos Costa
Departamento de Geología
Universidad Nacional de San Luis
E. de los Andes 950
5700 San Luis, Argentina
costa@unsl.edu.ar

Luca Guerrieri
Dipartimento per il Servizio Geologico d'Italia
Istituto Superiore per la Protezione e la Ricerca Ambientale
Via Vitaliano Brancati 48
00144 Rome, Italy
luca.guerrieri@isprambiente.it

James McCalpin
Geo-Haz Consulting, Inc.
600 East Galena Avenue
Crestone, Colorado 81131 U.S.A.
mccalpin@geohaz.com

Koji Okumura
Department of Geography, Faculty of Letters
Hiroshima University
1-3-2 Kagamiyama, Higashi-Hiroshima City
Hiroshima 739-8511, Japan
kojiok@hiroshima-u.ac.jp

Pilar Villamor
Earth Structure and Processes Department
GNS Science
1 Fairway Drive
5010 Lower Hutt, New Zealand
P.Villamor@gns.cri.nz

Published Online 16 October 2019

¹ Now at Université de la Sorbonne, Boulevard Saint Michel, 75005 Paris, France.